
CHALMERS
UNIVERSITY OF TECHNOLOGY

# Optimal design and operation of maritime energy systems based on renewable methanol and closed carbon cycles

Energy Conversion and Management 269 (2022) 116064

Contents lists available at ScienceDirect

Energy Conversion and Management

journal homepage: www.elsevier.com/locate/enconman

# Optimal design and operation of maritime energy systems based on renewable methanol and closed carbon cycles

Bernhard Thaler [a,*], Fayas Malik Kanchiralla [c], Stefan Posch [a], Gerhard Pirker [a], Andreas Wimmer [b], Selma Brynolf [c], Nicole Wermuth [a]

[a] Large Engines Competence Center, Graz, Austria
[b] Graz University of Technology, Institute of Thermodynamics and Sustainable Propulsion Systems, Austria
[c] Chalmers University of Technology, Department of Mechanics and Maritime Sciences, Sweden

ARTICLE INFO

*Keywords:*
Renewable fuels
Carbon capture
Sustainable shipping
Energy system optimization
Ship energy system

ABSTRACT

The phasing out of fossil fuels in the shipping sector is of key importance for reducing greenhouse gas emissions. Synthetic fuels based on renewable energy are a promising option for a sustainable maritime sector, with renewable methanol being one of the most widely considered energy carriers. However, the availability of renewable methanol is still limited and the costs associated with it are significantly higher than for conventional fuels, also because fuel synthesis must rely on carbon dioxide as a resource. Through the use of onboard carbon capture, the release of carbon dioxide during combustion can be avoided, and this closed cycle reduces the need for carbon sources. This paper investigates such a scenario by analyzing overall ship energy systems that use internal combustion engines with connected pre-combustion and post-combustion carbon capture technologies. The effect of these technologies on the techno-economic performance of a fully renewable energy system is investigated by setting up a mixed-integer optimization framework for the optimal design and operation of ship propulsion systems. The propulsion demand for the chosen case study consists of a typical operational profile of a ferry operating in the Baltic Sea. Comparison of the capture cases to a system solely based on renewable methanol reveals significant cost advantages of the closed carbon cycle systems. The baseline scenario has nearly 20% lower annual costs, with total capture rates of 90% in the post-combustion case and around 40% in the pre-combustion case. An extensive sensitivity analysis shows that these cost advantages are robust against various technological and economic boundary conditions. In the pre-combustion case, process heat demand reduction in combination with increased engine heat supply might enable higher capture rates beyond 90%. The results indicate that combining renewable fuels with onboard carbon capture creates opportunities for cost-effective, sustainable shipping.

## 1. Introduction

Deep decarbonization of the shipping industry is a major challenge in global efforts to combat climate change. To reach the targets of the International Maritime Organization (IMO), operational and technical measures aimed at increased energy efficiency need to be combined with the introduction of alternative marine fuels with low or zero greenhouse gas emissions and/or carbon abatement technologies [1–4]. There exists a range of different operational and technical energy efficiency measures including slow steaming, weather routing, propeller and propulsion maintenance and upgrades, and hull coating and maintenance [5,6]. A variety of possible alternative energy carriers are suggested, e.g., renewable methanol (Re-MeOH), hydrotreated vegetable oil and other renewable diesel, liquefied biogas, hydrogen ($H_2$), ethanol, ammonia, wind power, and electricity. Their potential for marine applications depends on their characteristics in terms of, for example, technical maturity and performance, environmental impact and cost [1,7–9]. The prerequisites for the fuel options also vary depending on the shipping segment and their potential is related to developments in other transportation and energy sectors. The fuel can be combined with different propulsion technologies such as internal combustion engines (including dual fuel engines) or different types of fuel cell technologies and exhaust abatement technologies, such as carbon capture.

Carbon capture is a widely researched and employed technique in onshore applications to reduce stationary power plant emissions, and is seen as a viable decarbonization option in the maritime sector [10].

* Corresponding author.
*E-mail address:* bernhard.thaler@lec.tugraz.at (B. Thaler).

https://doi.org/10.1016/j.enconman.2022.116064
Received 13 April 2022; Received in revised form 13 July 2022; Accepted 25 July 2022
Available online 23 August 2022

## Nomenclature

### Acronyms

| | |
|---|---|
| BECCU | Bioenergy carbon capture and usage |
| CAPEX | Capital expenditures/investment costs |
| $CO_2$ | Carbon dioxide |
| DAC | Direct air capture |
| $H_2$ | Hydrogen |
| ICE | Internal combustion engine |
| $LCO_2$ | Liquid carbon dioxide |
| LNG | Liquefied natural gas |
| MeOH | Methanol |
| MGO | Marine gas oil |
| MILP | Mixed integer linear programming |
| OPEX | Operational expenditures/operating costs |
| post-CCC | Post-combustion carbon capture |
| pre-CCC | Pre-combustion carbon capture |
| Re-MeOH | Renewable methanol |
| SOS | Special ordered set |
| WHR | Waste heat recovery |

### Decision variables

| | |
|---|---|
| $\boldsymbol{b}_{\mathbf{engine},\mathbf{H_2},\mathbf{t}}$ | Binary decision variable for each engine, defining if $H_2$ is combusted at time t |
| $\boldsymbol{C}_{\mathbf{s,t}}$ | Charge of storage s at time t |
| $\boldsymbol{CP}_{\mathbf{s}}$ | Storage unit capacity |
| $\boldsymbol{E}_{\mathbf{c,c',t}}$ | Energy flow from component c to component c′ at time step t |
| $\boldsymbol{i}_{\mathbf{c,t}}$ | Binary decision variable defining if converter c is operating at time t |
| $\boldsymbol{i}_{\mathbf{s,t}}$ | Binary decision variable defining if storage is being charged at time t |
| $\boldsymbol{m}_{\mathbf{c,c',t}}$ | Mass flow from component c into component c′ at time step t |
| $\boldsymbol{n}_{\mathbf{c,t}}$ | Binary decision variable defining if engine c is operating at time t |
| $\boldsymbol{P}_{\mathbf{c}}$ | Converter (input) power |
| $\boldsymbol{S}_{\mathbf{i,c,t}}$ | SOS type-2 decision variable for efficiency curve of converter c at segment i and time t |
| $\boldsymbol{T}_{\mathbf{c,t}}$ | Auxiliary decision variable to enable zero output of engine c at time t |

### Parameters

| | |
|---|---|
| $\Delta p_{\max,c}$ | Maximum specific power ramp of converter c |
| $\Delta t$ | Time resolution |
| $\dot{m}_{\text{exhaust}}$ | Exhaust mass flow rate |
| $\dot{m}_{\text{fuel}}$ | Fuel mass flow rate |
| $\eta_{c'c''}$ | Efficiency of converter c′ for energy flow into component c″ |
| $\eta_{c'}$ | Efficiency of converter c′ |
| $\eta_{\text{roundtrip,s}}$ | Roundtrip efficiency of storage s |
| $\lambda$ | Excess air ratio |
| $crf$ | Capital recovery factor |
| $f^{\text{E}}_{cc'}$ | Energy balance factor from component c to c′ |
| $f^{\text{m}}_{cc'}$ | Mass balance factor from component c to c′ |
| $f_{\text{s}}$ | Specific fuel cost of storage s |
| $h(T_{\text{exh}}, \lambda)$ | Specific exhaust gas enthalpy |
| $i$ | Inflation-free interest rate |
| $i*$ | Nominal interest rate |
| $I_{\text{c}}$ | Investment costs of component c |
| $l_{\text{c}}$ | Lifetime of component c |
| $n_{\text{r}}$ | Number of component replacements |
| $O^{\text{fix}}_{\text{c}}$ | Fixed operating costs of component c |
| $O^{\text{var}}_{\text{c}}$ | Variable operating costs of component c |
| $P^{lim,low}_{\text{c}}$ | Lower limit of $\boldsymbol{P}_{\mathbf{c}}$ in optimization |
| $P^{lim,up}_{\text{c}}$ | Upper limit of $\boldsymbol{P}_{\mathbf{c}}$ in optimization |
| $p^{min}_{\text{c}}$ | Minimum specific power of converter c |
| $P_{\text{D,t}}$ | Power demand at time t |
| $R_{\text{c}}$ | Replacement costs of component c |
| $S_{\text{c}}$ | Salvage incomes of component c |
| $SOC^{max}_{\text{s}}$ | Maximum state of charge of storage s |
| $SOC^{min}_{\text{s}}$ | Minimum state of charge of storage s |
| N | Project duration |

Though there are few systems in operation for onboard application, this market is changing fast and even first commercial applications are emerging [11]. Three carbon capture strategies are mostly discussed: post-combustion carbon capture (post-CCC), pre-combustion carbon capture (pre-CCC), and oxyfuel combustion. This publication focuses on onboard application of post-CCC and pre-CCC technology; the following paragraph provides a brief summary of related research.

Post-CCC is the most mature technology, and multiple stationary application examples exist [12]. Applied technologies mostly use chemical solvents (e.g., amine-based) to bind the $CO_2$ in an absorber column, followed by the regeneration of the solvent in a stripper column using thermal energy of an external source. The greatest advantage of post-CCC is its ability to retrofit already existing setups. On ships, for example, the exhaust gas thermal energy may be utilized to power the energy-intensive regeneration process. Captured $CO_2$ would then be compressed, liquefied and stored in onboard tanks until off-loading occurs. Several conceptual studies investigate such a post-CCC scenario for ship energy systems. In these studies a special emphasis has been placed on thermal energy demand to enable sufficient solvent regeneration and hence high capture rates. Luo and Wang [13] performed process simulations and techno-economic assessments for solvent-based onboard carbon capture. By using engine exhaust energy on a retrofitted cargo ship, a 73% capture rate could be achieved at a total cost of 78 €/$t_{CO_2}$. By adding additional energy sources, it was possible to increase the capture rate to 90% at a cost of 163 €/$t_{CO_2}$, related to increased fuel consumption. Feenstra et al. [14] performed process simulations for case studies of a diesel-fueled ship and a liquefied natural gas (LNG)-fueled ship and various combinations of carbon capture parameters. Depending on the chosen solvent, fuel, ship type and desired capture rate, $CO_2$ abatement costs between 98 and 389 €/$t_{CO_2}$ were retrieved, and the available thermal energy was mostly sufficient to drive the process. Building on the parameters for the diesel-fueled ship, Long et al. [15] performed detailed variations in solvent composition and optimized heat integration to further improve total $CO_2$ capture. For the most advanced configuration, capture rates as high as 94.7% were predicted. Ros et al. [16] evaluated the integration of post-CCC technology on LNG-fueled vessels in course of the DerisCO2 project including a detailed concept study of the Sleipnir ship. Not only exhaust gas heat integration but also final $CO_2$ pressure and LNG liquefaction capacity were found to be possible limiting factors of total capture rates. In the case of the example, maximum capture rates of 72.5% could be estimated, using LNG vaporization alone as the cooling source for $CO_2$ liquefaction. Einbu et al. [17] carried out detailed parametric studies with a data-driven process simulator applied to $CO_2$

transport ships. They found that the thermal energy demand for high capture rates can only be met by using additional fuel afterburners as a result of low thermal energy in the exhaust gas. A recent report published by the Oil and Gas Climate Initiative together with Stena Bulk [10] deemed onboard carbon capture to be generally feasible. However, the Suezmax tanker at the focus of the chosen case study would need significant additional equipment to increase capture rates due to the low exhaust heat availability of the large two-stroke engines.

Pre-CCC and its standard technology rely on a process similar to that of post-CCC. Instead of $CO_2$-rich exhaust gas, synthesis gas (CO + $H_2$) obtained from fuel reforming before combustion is converted to $CO_2$ and $H_2$ using thermal energy. $CO_2$ is then separated by e.g. an amine-solvent based absorber [18], and $H_2$ is used as the fuel for the combustion process. Even though the thermal energy demand for the capture process itself is lower than for post-CCC because of much higher partial pressures of $CO_2$, the energy demand of the entire process is higher due to the endothermic reforming reaction. As an alternative, fuel reformation and $CO_2$ separation can be jointly performed in a catalytic membrane reactor, as suggested within the HyMethShip project [19]. Instead of methane, methanol (MeOH) serves as the source of synthesis gas, which has the advantage of easier handling on board than LNG since the fuel has storage properties similar to those of conventional fossil liquids. In addition, the necessary reforming temperature and therefore energy demand are lower. If thermal energy demands for reforming can be fully met by the engine exhaust energy, increased total efficiencies can also be expected as a consequence of the higher chemical energy content of $H_2$ compared to MeOH.

Previously studied applications of onboard carbon capture focus mostly on fossil fuels. However, the use of renewable fuels makes it possible to keep carbon flows in a closed cycle by storing carbon dioxide ($CO_2$) on board and recycling it again on shore for fuel synthesis. If the renewable fuel is synthesized using non-fossil carbon sources, the propulsion concept would be inherently carbon neutral, even if a 100% capture rate could not be reached. Besides technological challenges, important questions remain such as whether such systems can be economically viable, and how they would be integrated into and affect the overall design of the ship propulsion system.

To evaluate and compare future decarbonization options on ships, studies mainly focus on single or just a small number of load operation points. The technological details of energy systems are either kept simple for the benefit of broad and comprehensive techno-economic assessments [20–23] or mapped in more detailed process simulations, which allows accurate technological insights into partial aspects of the energy system [14,24]. However, increased hybridization and the complex interplay of components that convert and store different forms of energy require more holistic strategies that are able to fully model the overall energy system. One approach to reaching these goals involves optimization via deterministic mathematical models that include full operational demand profiles. Such models are widely used in onshore power system modeling [25] and are also increasingly applied to optimize the design and operation of ship energy systems [26]. Baldi et al. [27] used mixed integer linear programming (MILP) to find the optimal load allocation of a cruise ship's energy system by taking into consideration propulsion, heat and electricity loads. In subsequent studies, the approach was used to study the optimal integration of solid oxide fuel cells into the ship's energy system [28] and to conduct comparative studies of future sustainable technology options based on economic optimizations [29]. Pivetta et al. [30] used MILP to determine the optimal design and operation of a fuel cell/battery hybrid energy system, with a focus on multi-objective minimization of costs and fuel cell degradation. Tang et al. [31] performed optimizations of load allocation in combination with a model-predictive control scheme to minimize total costs during cold-ironing connection. Bordin et al. [32] developed a MILP tool for choosing the optimal type and size of onboard battery storage systems based on operational profiles and safety related aspects. With the MILP approach, Yan et al. [33] undertook a multi-objective design and operation optimization of a cruise ship, to study the effect of component sizing on both total costs and onboard volume/weight. Besides these deterministic approaches, stochastic (metaheuristic) methods have also been employed for similar objectives in maritime energy systems. Techniques that are used include genetic algorithms [34–36] and particle swarm optimization [37].

This paper is the first to examine the optimal design and operation of onboard carbon capture in combination with renewable fuels in a ship energy system and its economic viability. A future scenario is investigated in which onboard carbon capture is embedded in a closed $CO_2$ cycle. $CO_2$ is captured from conversion of renewable methanol (Re-MeOH). In contrast to most other studies, $CO_2$ is not destined for long term storage but intended to be reused to synthesize Re-MeOH. MILP, which fully considers the complexity of such systems, is used to co-optimize design and operation. The ship energy system is modeled as a system of abstract components, which exchange energy and mass flows based on technological constraints. The approach allows modeling the entire ship energy system and its time-resolved performance, yielding a full operational profile during a voyage. Therefore, consideration of specific operation constraints, like maneuvers during port entry or on the open sea, is an inherent part of the assessment. An economic target function that accounts for all relevant investment and operating costs makes it possible to find the best system design under the given technological constraints.

Critical to the economic performance of such systems are feasible capture rates as well as achievable fuel cost savings through reduction of $CO_2$ costs by lowering the demand for alternative sources such as biomass or direct air capture. The techno-economic performance of these systems is analyzed by setting up models for an exemplified post-CCC and pre-CCC use case and comparing them to a fossil fuel baseline case and a Re-MeOH case without carbon capture. The chosen carbon capture technologies are an amine-solvent based system as the post-CCC application and the HyMethShip [19] configuration of steam reformation in a membrane reactor as the pre-CCC application. The influence of technological and economic assumptions are closely checked in a sensitivity analysis.

## 2. System description and optimization problem formulation

A RoPax ferry with a typical operating profile for a sea voyage was selected as case study. The ship operates on the Baltic Sea, is 240 m long, and has 51,837 gross tonnage. Four different concepts for a complete new propulsion system are compared with regard to energy supply (see Table 1): a fossil fuel baseline using marine gas oil (MGO; case a), a hybrid system using renewable methanol (Re-MeOH; case b), and two hybrid systems with a closed carbon cycle, one pre-CCC and one post-CCC, both of which are based on Re-MeOH (cases c and d). MGO is chosen as fuel in the fossil baseline case, as the Baltic Sea is part of an emission control area where the maximum allowed sulphur content in the fuel is 0.1% if no alternative measures to reduce sulphur emissions, such as exhaust gas cleaning systems, are employed. Fig. 1 shows schematics of the configurations that include all system components as well as relevant energy and mass flows. In all the configurations, four internal combustion engines generate the primary propulsion energy and supply the power demand via two gearboxes and propellers. Gearboxes are connected to electric machines and can exchange electric energy with an onboard battery storage system. Operation is limited by technological constraints and the conversion ratios of the different energy forms. The sizes as well as the deployment of the different technologies are optimized with respect to minimal annual system cost. Each energy system has to deliver the characteristic propulsion demand profile (Fig. 2) at the ship propellers at each time step of the investigated period. The profile is representative of a typical ferry voyage, including maneuvering at the origin and destination as well as on the open sea.

**Table 1**
Overview of the investigated configurations.

| | Configuration | Details |
|---|---|---|
| Case a | Fossil fuel-powered system | Engines use conventional marine gas oil (MGO) without any supplementary components. |
| Case b | Re-MeOH hybrid | Engines use renewable methanol (Re-MeOH) and are connected to the onboard electric system via gearboxes and electric machines. Energy can be stored in a battery storage system. |
| Case c | Re-MeOH with pre-combustion carbon capture (pre-CCC) | Re-MeOH is reformed to hydrogen ($H_2$) using exhaust gas thermal energy. Engines run flexibly on either $H_2$ or MeOH. $CO_2$ is separated in a membrane reformer, liquefied, and stored on board. |
| Case d | Re-MeOH with post-combustion carbon capture (post-CCC) | $CO_2$ from burned MeOH is captured via amine solvent-based absorption, using thermal energy from the exhaust gases for solvent regeneration. $CO_2$ is liquefied and stored on board. |

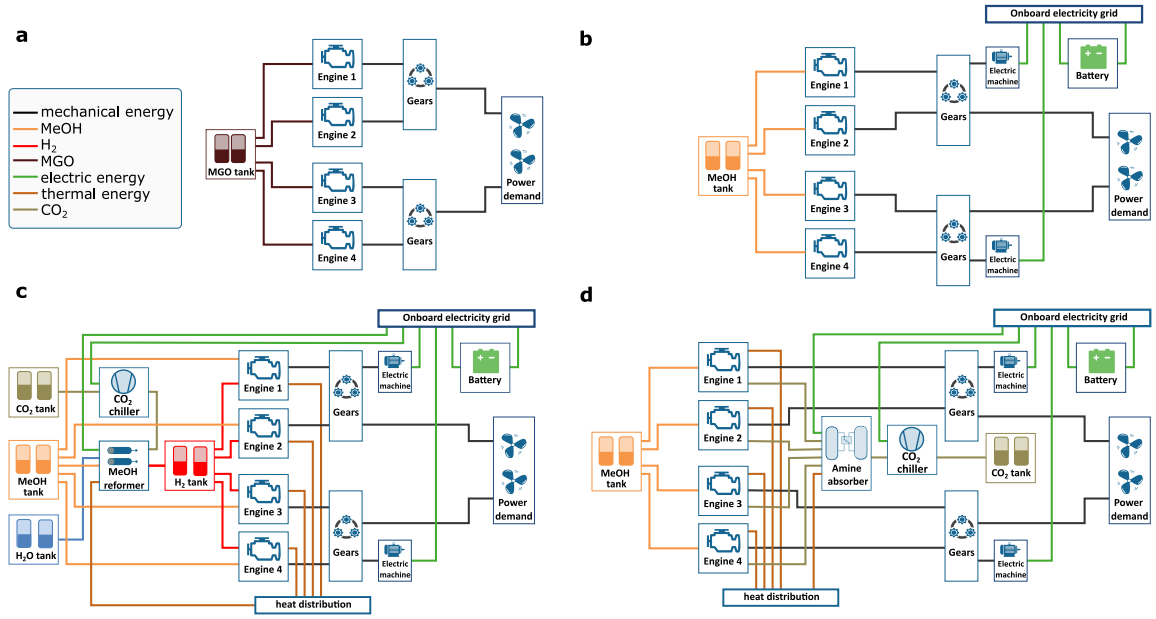


**Fig. 1.** Investigated energy system configurations. The four cases are a fossil fuel-based system (a), a hybrid system using Re-MeOH (b), a $H_2$/Re-MeOH based system with pre-combustion carbon capture (c), and a Re-MeOH based system with post-combustion carbon capture (d).

### 2.1. Objective function and decision variables

System optimization is implemented via MILP using Python-MIP [38] and the open-source solver CBC [39]. The systems consist of energy components that are roughly grouped into energy storage units and converters. Components exchange energy and mass flows based on their efficiencies and technological constraints. Continuous decision variables are the nominal sizes of all components (converter powers $\boldsymbol{P_c}$ and storage capacities $\boldsymbol{CP_s}$) as well as the energy and mass flows of all connections and time steps $\boldsymbol{E_{c,c',t}}$, which denotes the energy flow from component c to component c′ at time t. Several integer decision variables are included as auxiliary variables needed for constraints. Target function is the annualized total system cost, which consists of annualized specific capital expenditures ($I_c$/CAPEX), replacement costs ($R_c$) and end-of-project salvage costs ($S_c$), fixed and variable operating expenditures ($O_c^{fix}$/OPEX and $O_c^{var}$, respectively), and variable storage fuel costs $F_s$.

$$\text{Annual costs} = \sum_{c} \left[ \left( I_c + R_c - S_c \right) \cdot crf + O_c^{fix} \right] \cdot \boldsymbol{P_c} + \sum_{c,c',t} O_c^{var} \cdot \boldsymbol{E_{c,c',t}} + \sum_{s} F_s \tag{1}$$

The specific variable operational expenditures of each component are multiplied by the actual energy flow at each time step; the specific investment and fixed operational costs are multiplied by the component size. The capital recovery factor $crf$ is defined as

$$crf = \frac{i \cdot (1+i)^N}{(1+i)^N - 1}, \tag{2}$$

where $N$ is the assumed project duration and $i$ is the inflation-free interest rate that is calculated from the nominal interest rate $i^*$ and expected inflation rate $f$ with:

$$i = \frac{i^* - f}{1 - f}. \tag{3}$$

Net annual costs are therefore the same as the product of $crf$ and net present value [40]. Specific replacement costs $R_c$ and salvage costs $S_c$ are defined as in [41]:

$$R_c = \sum_{m=1}^{n_r} \frac{I_c}{(1+i)^{m \cdot l_c}} \tag{4}$$

$$S_c = \frac{I_c}{(1+i)^N} \cdot \frac{l_c \cdot (1+n_r) - N}{l_c}, \tag{5}$$

where $n_r$ is the number of replacements for each component, calculated by $N/l_c$. The optimization time span consists of a representative voyage of 17 h with a time resolution of 15 min. The annualized costs of voyage dependent parameters such as fuel costs are obtained by extrapolating the obtained data to a one year time span, assuming 70 % utilization of the propulsion demand profile over the full year, which is equivalent to one voyage per day.

The following sections describe the technological specifications and constraints for the components in relation to the converters and storage units. The characteristic technological parameters for the individual technologies are summarized in Table 2.

### 2.2. Energy converters

Energy converters are characterized by input and output flows (energy and/or mass), which are converted into each other by employing

**Table 2**
Technological data used to describe components. All specific energies and efficiencies related to fuels are based on lower heating values.

| Components | Conversion factors | | $\Delta p_{max}$ (%/h) |
|---|---|---|---|
| Engines | Efficiency maps (Fig. 3) | | – |
| Electric machine | $\eta_{elec}$ | 95% | – |
| Battery | $\eta_{roundtrip}$ | 90% | – |
| Gearbox | $\eta_{mech}$ | 97% | – |
| Membrane reformer | Inputs | 1.0 $kWh_{MeOH}$ | 100 |
| | | 0.25 $kWh_{therm}$ | |
| | | 0.005 $kWh_{el}$ | |
| | Outputs | 1.13 $kWh_{H_2}$ | |
| | | 0.236 $kg_{CO_2}$ | |
| | | ($\eta_{capture}$ = 95%) | |
| Amine carbon capture | Inputs | 1.0 $kg_{CO_2}$ | 100 |
| | | 0.85 $kWh_{therm}$ | |
| | | 0.077 $kWh_{el}$ | |
| | Outputs | 0.9 $kg_{CO_2}$ | |
| | | ($\eta_{capture}$ = 90%) | |
| $CO_2$ liquefaction | Demand | 0.03 $kWh_{el}/kg_{CO_2}$ | – |

specific efficiencies or conversion factors. The decision variables of the converters are constrained by the following conditions:

- Converters are modeled using either linearized efficiency curves (see below) or energy and mass balances with constant conversion ratios over the full load range. In the simplest case in which a converter c′ converts energy between two specific energy forms, the sum of all input and output energy flows of the connected components are equated via the converter efficiency $\eta_{c'}$:

$$\sum_{c} \boldsymbol{E}^{in}_{c,c',t} = \sum_{c''} \boldsymbol{E}^{out}_{c',c'',t} / \eta_{c'} \tag{6}$$

An example of this case is an electric motor, which transforms electrical energy into mechanical energy with constant efficiency. Note that this equation is not an energy conservation balance as the system losses (1-$\eta_{c'}$) are virtually transferred out of the system. In the case in which several different types of output energy participate, the correct conversion ratios are described by multiple efficiencies $\eta_{c'c''}$:

$$\sum_{c} \boldsymbol{E}^{in}_{c,c',t} = \sum_{c''} \boldsymbol{E}^{out}_{c',c'',t} / \eta_{c'c''} \tag{7}$$

An example of several different types of output energy is an engine with load-independent efficiencies for mechanic and thermal output. If a converter transforms several input energies to several output energies, the correct input energy conversion factors must also be specified:

$$\sum_{c} \boldsymbol{E}^{in}_{c,c',t} / f^{E}_{cc'} = \sum_{c''} \boldsymbol{E}^{out}_{c',c'',t} / f^{E}_{c'c''} \tag{8}$$

An example of this is the MeOH reformer, which converts chemical (MeOH) and thermal energy as inputs to chemical energy as output ($H_2$). The factors $f^{E}_{cc'}$ relate the correct balance of required thermal energy per chemical energy of MeOH (cf. Table 2). Note that Eqs. (6) and (7) are special cases of Eq. (8), where all $f^{E}_{cc'}$ are set to 1. If not only energy flows but also mass flows are involved, Eq. (8) must also hold true for the corresponding energy-to-mass conversion factors $f^{m}_{c'c''}$:

$$\begin{aligned} \sum_{c} \boldsymbol{E}^{in}_{c,c',t} / f^{E}_{cc'} &= \sum_{c''} \boldsymbol{m}^{out}_{c',c'',t} / f^{m}_{c'c''} \\ \sum_{c} \boldsymbol{m}^{in}_{c,c',t} / f^{m}_{cc'} &= \sum_{c''} \boldsymbol{E}^{out}_{c',c'',t} / f^{E}_{c'c''} \end{aligned} \tag{9}$$

Once again, an example of this is the membrane reformer: In addition to chemical energy output ($H_2$), a $CO_2$ mass flow is produced, which relates to MeOH input with the conversion ratio $f^{m}_{c'c''}$ = 0.236 $kg_{CO_2}/kWh_{MeOH}$, defined by the carbon content of methanol and the capture rate.

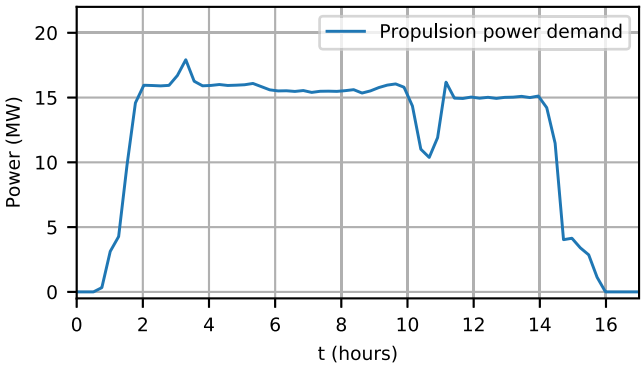


**Fig. 2.** Representative propulsion power demand profile for a single voyage.

- The sum of energy flows into each component cannot exceed the maximum input power of the component $\boldsymbol{P}^{max}_{c}$:

$$\sum_{c'} \boldsymbol{E}^{in}_{c',c,t} \le \boldsymbol{P}^{max}_{c} \cdot \Delta t \tag{10}$$

Note that $\boldsymbol{P}^{max}_{c}$ is defined at the input side of each component. For example, this value for engines describes the maximum fuel load. The time resolution $\Delta t$ is necessary for the conversion between energy and power.

- To account for reduced transient capabilities, converters can be constrained in their maximum dynamic load change:

$$\sum_{c'} \boldsymbol{E}^{in}_{c',c,(t+1)} - \sum_{c'} \boldsymbol{E}^{in}_{c',c,t} \le \boldsymbol{P}^{max}_{c} \cdot \Delta p_{max,c} \cdot \Delta t \tag{11}$$

$\Delta p_{max,c}$ is the maximum specific power step.

- If an energy converter has a nominal minimum power rating $p^{min}_{c}$, an auxiliary binary variable $\boldsymbol{i}_{c,t}$ is introduced to indicate whether the converter is operating:

$$\begin{aligned} \sum_{c'} \boldsymbol{E}^{in}_{c',c,t} &\ge \left[ \boldsymbol{P}^{max}_{c} - \left(1 - \boldsymbol{i}_{c,t}\right) \cdot P^{lim,up}_{c} \right] \cdot p^{min}_{c} \cdot \Delta t \\ \sum_{c'} \boldsymbol{E}^{in}_{c',c,t} &\le \boldsymbol{i}_{c,t} \cdot P^{lim,up}_{c} \cdot \Delta t \end{aligned} \tag{12}$$

$P^{lim,up}_{c}$ is the manually chosen upper limit for the decision variable $\boldsymbol{P}^{max}_{c}$ for the optimization. The binary variable $\boldsymbol{i}_{c,t}$ is necessary so that the converter output may be zero.

- Energy flows to the propellers have to match the demand profile $P_{D,t}$ at all time steps (Fig. 2):

$$\sum_{c'} \boldsymbol{E}^{in}_{c',D,t} = P_{D,t} \cdot \Delta t \tag{13}$$

### 2.2.1. Engines

Internal combustion engines are modeled based on their efficiency maps for mechanical and thermal outputs. In this section, mechanical efficiency refers to the useful output of mechanical energy, and thermal efficiency to useful thermal energy, in both instances relative to fuel energy. Since efficiency data for engines operated with $H_2$ and MeOH fuels is still rare, data for natural gas and MGO engines, respectively, is used. This approach is considered valid because $H_2$ and natural gas combustion face similar obstacles such as knocking combustion, and future developments are expected to achieve similar efficiencies and combustion performance. Efficiency curves were obtained from four-stroke engine manufacturer data for a representative diesel engine [43] and gas engine [42] that is publicly available and shown in Fig. 3a. Note that these engines were not designed for enhanced thermal energy output, so their operation might not be ideal for carbon capture applications. Outcome sensitivities related to thermal as well as mechanical efficiencies are therefore closely evaluated in Section 3.4.

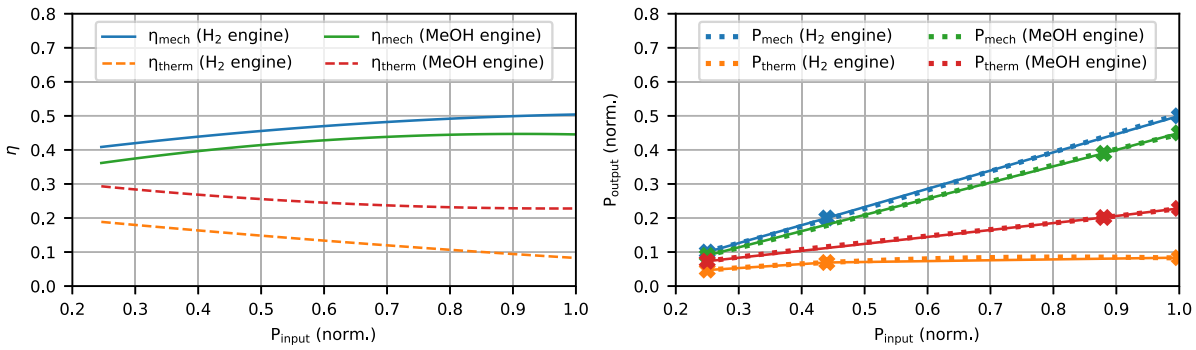


**Fig. 3.** Engine efficiency maps. (a) Mechanical and thermal efficiencies as function of normalized input power for a Wärstilä 8V31SG (natural gas and $H_2$, respectively) [42] and a Wärtsilä 12V26F (MGO and MeOH, respectively) [43]. (b) Output powers as a function of input powers (dotted line), together with piecewise linearized segments used for the optimization (continuous line). Markers indicate the fixed segment edges ($E^{\text{in}}_{i,c}$, $E^{\text{out}}_{i,c}$).

Available thermal efficiencies for the carbon capture heat demands are calculated based on exhaust gas temperatures ($T_{\text{exh}}$, after turbocharger) specified on engine manufacturer datasheets. Between 25% and 100% load, exhaust gas temperatures lie between 411 and 344 °C for the gas ($H_2$) engine [42] and between 367 and 343 °C for the diesel (MeOH) engine [43]. For the MeOH-reformer (case c), a catalyst temperature level of 280 °C is assumed based on membrane reformer simulations from the HyMethShip project. It is assumed that the exhaust gas is cooled down to 245 °C ($T_{\text{exh,low}}$), at the low temperature return side of a counterflow heat exchanger. Thermal engine efficiencies are then determined using the exhaust mass flow rate $\dot{m}_{\text{exhaust}}$ based on complete combustion, and calculations of the specific exhaust gas enthalpies h(T, $\lambda$) using NASA polynomials [44]:

$$\eta_{therm} = \frac{\dot{m}_{\text{exhaust}}(\lambda) \cdot \left[h(T_{\text{exh}}, \lambda) - h(T_{\text{exh,low}}, \lambda)\right]}{\dot{m}_{\text{fuel}} \cdot LHV_{\text{H}_2/\text{MeOH/MGO}}}. \tag{14}$$

$LHV$ is the lower heating value of the respective fuel with mass flow rate $\dot{m}_{\text{fuel}}$. Excess air ratios ($\lambda$) used to calculate exhaust gas mass flow rates are estimated based on the specified input air and fuel flows and range from 2.0 to 2.5, for the natural gas and MGO engine, respectively. Here the thermal efficiency calculated refers to the deliverable carbon capture heat duty and not the possible overall thermal engine output.

The temperature of the thermal energy supply of the amine carbon capture plant (case d) is assumed to be lower, approximately 130 °C for reboiler steam generation, resulting in a return level of 80 °C at the heat exchanger [45]. The exhaust gas is assumed to be cooled to 100 °C, leading to larger thermal efficiencies compared to the reformer configuration due to better exploitation of available exergy (see Fig. 3b). The temperature levels of the remaining engine energy sources, for example cooling circuits, are too low for the required carbon capture processes. Though theses sources are not considered, they could still be exploited to supply onboard heat demands (e.g., hotel loads).

As efficiency curves are non-linear, piecewise linearization is performed. Efficiency maps are translated to curves describing the relationship between input and output power (Fig. 3b). In the first step, these curves are linearized using three segments. This level of discretization is considered sufficiently accurate and still computationally affordable. The positions of the edge points $E^{i}_{in}$ are found by minimizing the sum of squared residuals, as suggested in [46]. In the second step, special ordered sets (SOS) are used to describe the input/output constraint [47]: For each edge point $E^{\text{in}}_{i,c}$ of the piecewise linearized curve, an auxiliary continuous decision variable $\boldsymbol{S}_{\text{i,c,t}}$ is introduced at each time step:

$$\sum_{c'} \boldsymbol{E}^{\text{in}}_{\text{c,c',t}} = \sum_{\text{i}} \boldsymbol{S}_{\text{i,c,t}} \cdot E^{\text{in}}_{\text{i,c}} \tag{15}$$

$$\sum_{c'} \boldsymbol{E}^{\text{out}}_{\text{c,c',t}} = \sum_{\text{i}} \boldsymbol{S}_{\text{i,c,t}} \cdot E^{\text{out}}_{\text{i,c}} \tag{16}$$

Note that the points $E^{\text{in}}_{i,c}$ are given for a normalized curve. If multiple $E^{\text{out}}_{i,c}$ are present (e.g., mechanical and thermal energy), Eq. (16) must be fulfilled for all output streams. The pairs of $E^{\text{in}}_{i,c}$ and $\boldsymbol{S}_{\text{i,c,t}}$ are included as an SOS-type 2, which ensures that only two of the $\boldsymbol{S}_{\text{i,c,t}}$ can be greater than zero. If no minimum power is enforced, the following constraint guarantees that only allowed energy values are accepted:

$$\sum_{\text{i}} \boldsymbol{S}_{\text{i,c,t}} = \boldsymbol{P}^{max}_{\text{c}} \cdot \Delta t \tag{17}$$

Large engines are required to run above a certain minimum power threshold. This minimum power rating $p^{min}_{\text{c}}$ is enforced by limiting the lowest edge point of $E^{\text{in}}_{\text{i,c}}$ to this value. However, Eqs. (15) and (17) would then make it impossible for the energy flows to be zero. An additional continuous decision variable $\boldsymbol{T}_{\text{c,t}}$ and a binary decision variable $\boldsymbol{n}_{\text{c,t}}$ are introduced to enable cases with zero converter output:

$$\boldsymbol{T}_{\text{c,t}} = \begin{cases} \boldsymbol{P}^{max}_{\text{c}}, & \text{if } \boldsymbol{n}_{\text{c,t}} = 1 \text{ (converter “on”)} \\ 0, & \text{if } \boldsymbol{n}_{\text{c,t}} = 0 \text{ (converter “off”)} \end{cases} \tag{18}$$

Condition (18) is fulfilled via the following constraints:

$$\boldsymbol{T}_{\text{c,t}} \geq \boldsymbol{n}_{\text{c,t}} \cdot P^{lim,low}_{\text{c}} \tag{19}$$

$$\boldsymbol{T}_{\text{c,t}} \leq \boldsymbol{n}_{\text{c,t}} \cdot P^{lim,up}_{\text{c}} \tag{20}$$

$$\boldsymbol{T}_{\text{c,t}} \leq \boldsymbol{P}^{max}_{\text{c}} \tag{21}$$

$$\boldsymbol{T}_{\text{c,t}} \geq \boldsymbol{P}^{max}_{\text{c}} - \left(1 - \boldsymbol{n}_{\text{c,t}}\right) \cdot P^{lim,up}_{\text{c}} \tag{22}$$

$P^{lim,low}_{\text{c}}$ and $P^{lim,up}_{\text{c}}$ are the lower and upper optimization limits for $\boldsymbol{P}^{max}_{\text{c}}$, respectively, which are manually set for the optimization. Eq. (17) then takes the form:

$$\sum_{\text{i}} \boldsymbol{S}_{\text{i,c,t}} = \boldsymbol{T}_{\text{c,t}} \cdot \Delta t \tag{23}$$

Each configuration case is modeled using four engines. As is common in maritime energy systems, the maximum power of the engines is constrained to being identical for redundancy reasons:

$$\boldsymbol{P}^{max}_{\text{engine}_1} = \boldsymbol{P}^{max}_{\text{engine}_2} = \boldsymbol{P}^{max}_{\text{engine}_3} = \boldsymbol{P}^{max}_{\text{engine}_4} \tag{24}$$

To avoid convergence problems with ambiguous power dispatch, the order of the energy supply to meet the propulsion demand is manually set:

$$\boldsymbol{E}^{in}_{\text{engine}_1,\text{t}} \geq \boldsymbol{E}^{in}_{\text{engine}_2,\text{t}} \geq \boldsymbol{E}^{in}_{\text{engine}_3,\text{t}} \geq \boldsymbol{E}^{in}_{\text{engine}_4,\text{t}} \tag{25}$$

These engines are usually capable of ramping up to full load within less than one minute, so there are no transient limitations on engine operations given the time resolution of 15 min. In case c, engines are operated in a dual fuel mode and are capable of burning either $H_2$ or MeOH. For the sake of simplicity, the same efficiency curves are taken for both fuels. The following constraints ensure that each engine only burns either $H_2$ or MeOH:

$$\boldsymbol{E}^{in}_{\text{engine,H}_2,\text{t}} \leq \boldsymbol{b}_{\text{H}_2,\text{t}} \cdot 10^9 \tag{26}$$

$$\boldsymbol{E}^{in}_{\mathbf{engine,MeOH,t}} \leq \left(1 - \boldsymbol{b}_{\mathbf{H_2,t}}\right) \cdot 10^9 \quad (27)$$

where $\boldsymbol{b}_{\mathbf{H_2,t}}$ is a binary decision variable, which takes the value of one in the case of $H_2$ combustion. The number $10^9$ was chosen since it is sufficiently large enough not to limit energy flows.

#### 2.2.2. Membrane reformer/pre-combustion carbon capture

The MeOH-reformer for case c is modeled as a black box with specific input and output flows, see Table 2 for a summary. The component is thought to consist of multiple heat exchangers, which supply the necessary thermal energies, and the reformer itself, which consists of a catalyst bed and a carbon-based membrane where the catalytic reaction as well as product separation take place:

$$CH_3OH_{(g)} + H_2O_{(g)} \rightarrow 3H_2 + CO_2 \quad (\Delta H^0_{R298} = 49.2\ \mathrm{kJ/mol}) \quad (28)$$

As the technology is not yet widely employed in large scale systems, there is little data on energy requirements and efficiencies for the membrane reactor process in the literature and it strongly depends on the specific catalyst technology [48]. The total thermal energy demand is estimated from simulation data available from the HyMethShip project [19]. It consists of the necessary energy to vaporize and heat MeOH and $H_2O$ up to an assumed reaction temperature of 280 °C and the heat demand of the reaction itself. This energy demand is already reduced by using available condensation energy in the retentate. A complete reaction with 100 % conversion of MeOH to $H_2$ is assumed. As literature values for achievable $H_2$ purity under laboratory conditions range up to nearly 100% [48,49], a $CO_2$-capture efficiency of 95% is used. Electric auxiliaries, consisting mainly of pumps for the fluids, are assumed to consume 0.005 kWh per kWh MeOH. As the reformer is a thermally inert system, a maximum allowed power ramp of 100% per hour is chosen to limit transient capabilities (Eq. (11)), assuming hot starts. Long cold start times are not considered because it is assumed that the reformer is in standby-mode during loading and unloading at the ports.

#### 2.2.3. Amine post-combustion carbon capture

The carbon capture equipment for case d is an amine solvent-based carbon capture plant. It consists of an absorber, where $CO_2$ is absorbed by the solvent, and a stripper, where $CO_2$ is separated using thermal energy from a reboiler. Key figures for this technology are the capture efficiency, assumed to be 90% as in most studies [45], and the reboiler heat duty, assumed to be 0.85 $\mathrm{kWh/kg_{CO_2^{input}}}$ based on a range of reported literature values between 0.8 and 1.0 $\mathrm{kWh/kg_{CO_2^{input}}}$ [14,45,50,51]. Variations in capture efficiency and heat duty are considered in the sensitivity analysis (Section 3.5). $CO_2$ at the output is compressed prior to liquefaction to about 15 bar, at an electricity consumption of 0.05 kWh / $\mathrm{kg_{CO_2^{input}}}$ [14]. The electric energy demand for auxiliaries is assumed to be 0.027 $\mathrm{kWh/kg_{CO_2^{input}}}$. Literature values for flexibility of post-combustion carbon capture plants during operation indicate no limitation for the time resolution of 15 min chosen here. For example, Domenichini et al. [52] set no CCS imposed limitation on ramping rates for gas power plants, yet these plants require rather long (hot) start times, ranging from one to two hours. Therefore an allowed maximum power ramp of 100% nominal power per hour was chosen (Eq. (11)), in analogy to the membrane reformer.

#### 2.2.4. $CO_2$ liquefaction

$CO_2$ is stored on board in a liquefied state. The liquefaction process in both carbon capture cases is assumed to be identical. The energies required for liquefaction that are found in the literature range from 10 to 160 $\mathrm{kWh}/t_{CO_2}$, depending on the technology used as well as the initial and final temperatures and pressures [14,45,53–55]. A storage temperature of −30 °C at a pressure of 15 bar is assumed and documented energy demand values are used. Both the membrane reformer and the carbon capture plant are assumed to produce a stream of pure $CO_2$ at ambient temperature that is already pressurized. Energy demands for pressurization are included in the reformer/carbon capture electricity demands. The energy demand for subsequent $CO_2$ liquefaction of 30 kWh / $\mathrm{t_{CO_2^{input}}}$ is chosen based on [55].

**Table 3**
Project and specific fuel parameters; chemical energies are based on lower heating values.

| Parameter | Value | Reference |
|---|---|---|
| Currency | Euros (€) | |
| Base year for economic data | 2020 | |
| Project duration | 30 years | |
| Nominal interest rate | 5% | |
| Inflation rate | 1.25% | European average 2010–2020 |
| MGO cost | 35 €/$\mathrm{MWh_{chem}}$ | Cost during 12/2020 |
| MGO $CO_2$-intensity | 266 g/$\mathrm{kWh_{chem}}$ | [57] |
| Re-MeOH cost (baseline) | 180 €/$\mathrm{MWh_{chem}}$ | [58] |
| Re-MeOH $CO_2$-intensity | 249 g/$\mathrm{kWh_{chem}}$ | Equivalent to MeOH carbon content |
| $CO_2$ cost (baseline) | 250 €/$\mathrm{t_{CO_2}}$ | [58] |

### 2.3. Energy/mass storage units

Modeled storage units include MeOH (MGO) tanks, batteries, $CO_2$ tanks and $H_2$ tanks for case c. Storage units for water and chemicals are not considered. Storage units are parametrized through their maximum capacity $\boldsymbol{CP_s}$ and their maximum charge/discharge power $\boldsymbol{P_s}$. Storage unit charges $C_{s,t}$ are defined as:

$$C_{s,t} = C_{s,(t-1)} + \sum_{c'} \boldsymbol{E}^{in}_{\mathbf{c',s,t}} - \boldsymbol{E}^{out}_{\mathbf{s,c',t}} / \eta_{roundtrip}, \quad (29)$$

where $\eta_{roundtrip}$ is the roundtrip efficiency of the storage unit, which is assumed to be 90% for the battery [56] and 100% for the fuel storage units. Storage unit charge levels can be constrained to technical minimal state of charge ($SOC^{min}_c$) and maximal state of charge ($SOC^{max}_c$):

$$C_{s,t} \leq \boldsymbol{CP_s} \cdot SOC^{max}_c \quad (30)$$

$$C_{s,t} \geq \boldsymbol{CP_s} \cdot SOC^{min}_c \quad (31)$$

If simultaneous charge and discharge of an energy storage unit is technologically not possible (e.g., batteries), a binary decision variable $\boldsymbol{i}_{\mathbf{s,t}}$ is introduced to prevent input and output flows from being greater than zero at the same time:

$$\sum_c \boldsymbol{E}^{in}_{\mathbf{c,s,t}} \leq \boldsymbol{i}_{\mathbf{s,t}} \cdot 10^9 \quad (32)$$

$$\sum_c \boldsymbol{E}^{out}_{\mathbf{s,c,t}} \leq \left(1 - \boldsymbol{i}_{\mathbf{s,t}}\right) \cdot 10^9 \quad (33)$$

In the economic target function (Eq. (1)), variable fuel costs $F_s$ are calculated based on storage charge changes over the time span of the simulation:

$$F_s = \left(C_{s,t_{end}} - C_{s,t_0}\right) \cdot f_s \quad (34)$$

$f_s$ are the specific fuel costs of each fuel as specified in Table 3.

### 2.4. Economic data

Table 3 shows the assumed overall project parameters. Specific investment and operating costs for the technologies were obtained from the literature review and are summarized in Table 4. Values found in USD and GBP were calculated to EUR using exchange rates of 0.84 EUR/USD and 1.13 EUR/GBP, respectively (reference year 2020). All cost estimates are made for the year 2020. If the cost values in literature sources were in reference to a specific year (e.g. $\mathrm{USD_{2010}}$), prices were scaled to 2020 values by using the average inflation rate of

**Table 4**
Summary of economic data for the target function calculation with 2020 as the reference year for the values in €. Fixed annual operating costs (OPEX) are expressed as a percentage of investment costs (CAPEX). All specific costs related to fuels represent lower heating values (LHV).

| Component | CAPEX | OPEX fix | Lifetime | References | Comments |
|---|---|---|---|---|---|
| MGO engine | 240 €/$kW_{mech}$ | 2% | 30 years | [20] | |
| MeOH engine | 265 €/$kW_{mech}$ | 2% | 30 years | [20] | |
| $H_2$/MeOH engine | 470 €/$kW_{mech}$ | 2% | 30 years | [20] | |
| Exhaust gas WHR | 114 €/$kW_{mech}$ | 2% | 30 years | [59] | In optimization included in engine cost |
| Gearbox | 85 €/$kW_{mech}$ | 1% | 30 years | [20] | |
| Electric machine | 59 €/$kW_{el}$ | 1% | 30 years | [60] | |
| Membrane reactor | 520 €/$kW_{MeOH}$ | 2.5% | 9 years | [61–63] | Lifetime estimated based on assumed 60,000 operating hours and 70% yearly utilization |
| Amine carbon capture plant | 2200 €/$kg_{CO_2}$/h | 3% | 25 years | [14,45,64] | Additional variable OPEX of consumed amine solvent included (2.5 €/$t_{CO_2}$) |
| $CO_2$ liquefaction | 157 €/$kg_{CO_2}$/h | 10% | 30 years | [45,53–55] | Cost estimate based on liquefaction without compression |
| Battery | 236 €/$kWh_{el}$<br>219 €/$kW_{el}$ | 2.5% | 15 years | [56] | |
| MGO tank | 0.10 €/$kWh_{chem}$ | 2% | 30 years | [65] | |
| MeOH tank | 0.16 €/$kWh_{chem}$ | 2%- | 30 years | [65] | |
| $H_2$ tank | 27 €/$kWh_{chem}$ | 2% | 25 years | [66] | Pressurized hydrogen gas storage without compressor |
| $LCO_2$ tank | 0.95 €/kg | 5% | 20 years | [55] | |

1.25% of the period 2010–2020, as specified by the European Central Bank [67]. If no year was given, the year of publication submission was taken as the starting point.

For certain investment costs (Table 4), high uncertainties for cost estimates were present in the literature. Large cost ranges were found especially for technologies not yet fully mature (e.g., membrane reactors) and for those still experiencing cost reductions due to economics of scale (e.g., batteries). Multiple literature sources were compared and representative values were chosen for each of these components. For the amine carbon capture plant, multiple cost estimates are available for stationary, large scale power plant applications. Rubin et al. [68] give an extensive cost overview of various types of power plants relying on coal or natural gas. The global CCS institute [69] regularly provides an overview of carbon capture costs for non-power plant applications such as cement or iron and steel applications. Only a few descriptions of smaller scale shipping applications are found, mostly at the level of process simulation and design [14,70]. For the membrane reactor, even fewer cost estimates exist. As a result, the sensitivity analysis closely examines uncertainties in the cost of investments in both technologies (see Section 3.5).

Fuel cost estimates for the Re-MeOH and respective $CO_2$ capture costs shown in Table 3, were assessed from existing works. Brynolf et al. [71] found large ranges between 120 to 650 €/$MWh_{chem}$ in a broad literature study. They estimate a base cost of 210 €/$MWh_{chem}$, however at a relatively low $CO_2$ cost of 30 €/$_{t_{CO_2}}$. In a sensitivity case for 2020 and 2030, Re-MeOH costs on the basis of DAC were estimated to be 470 and 280 €/$MWh_{chem}$ with $CO_2$ costs of 1000 and 500 €/$t_{CO_2}$ (52% and 43% cost share), respectively. Horvath et al. [21] made cost estimates of various renewable fuels based on best case locations with high potentials of low-cost renewables (wind, solar), estimating a value of 88 €/$MWh_{chem}$ for Re-MeOH in 2030. Based on a case study of the production of synthetic natural gas (SNG), Fasihi et al. [72] estimated DAC costs of 225 €/$t_{CO_2}$ (100 €/$t_{CO_2}$ in 2030), resulting in a DAC cost share of 27% (2030: 21%) in the whole power-to-gas process. The International Renewable Energy Agency (IRENA) [58] estimates the cost of Re-MeOH based on DAC synthesis to be between 180 and 360 €/$MWh_{chem}$ (2021) with a DAC cost between 250–500 €/$t_{CO_2}$, making up a 35% $CO_2$ cost share. The Swiss company *Climeworks* claims current (2021) $CO_2$ capture costs are around 500 €/$t_{CO_2}$ for their demonstration plants [73] with the target of reaching at least 250 €/$t_{CO_2}$ by 2030, when the technology scales. Apart from $CO_2$, the largest contributions to Re-MeOH costs are made up by renewable electricity costs and investment costs for the electrolyzer. Therefore all major cost contributions to Re-MeOH including $CO_2$ capture costs, are expected to be driven down by future economies of scale, resulting in even greater cost uncertainties in current modeling. Here values of 180 €/$MWh_{chem}$ and 250 €/$t_{CO_2}$ are chosen as a baseline cost estimate based on the lower margin of the IRENA estimation. To test the influences of higher costs and possible decreases in future costs, detailed changes in the cost of Re-MeOH and $CO_2$ capture are covered by the sensitivity analysis (see Sections 3.2 and 3.3).

**Table 5**
Optimized component sizes and results for the baseline scenarios.

| | Case a (MGO) | Case b (Hybrid) | Case c (Pre) | Case d (Post) |
|---|---|---|---|---|
| Battery power (MW) | – | 2.11 | 0.50 | 2.38 |
| Battery capacity (MWh) | – | 0.89 | 0.14 | 2.02 |
| Engine ($MW_{mech}$) | 4.57 | 4.07 | 4.56 | 4.26 |
| Electric machine (MW) | – | 1.05 | 0.55 | 2.96 |
| Reformer ($MW_{chem}$) | – | – | 11.82 | – |
| Amine plant ($t_{CO_2,in}$/h) | – | – | – | 9.48 |
| $CO_2$ tank (t) | – | – | 37.71 | 110.87 |
| MGO/MeOH tank (MWh) | 469.38 | 465.83 | 406.55 | 496.72 |
| $H_2$ tank (MWh) | – | – | 1.87 | – |
| $CO_2$ chiller ($t_{CO_2}$/h) | – | – | 2.79 | 8.54 |
| Annual costs (M€) | 6.37 | 30.77 | 24.92 | 25.22 |
| Captured $CO_2$ (%) | – | – | 37.26 | 90.0 |

Note that this analysis compares different fully renewable energy systems. $CO_2$ costs are prices for the commodity $CO_2$ based on direct air capture, not carbon taxes added to scenarios with fossil energy carriers. Comparisons of the renewable scenarios (cases b–d) to the fossil baseline case (case a) are therefore comparisons to the status quo without carbon taxation in the maritime industry. However, comparative carbon prices will be assessed in the sensitivity analysis to check how renewable energy scenarios compare to the status quo including carbon taxation.

## 3. Results

This section first describes the optimized results of baseline scenarios with techno-economic input data as shown in Tables 2 and 4. Following the baseline results, it presents several sensitivity cases with systematic changes in specific parameters.

### 3.1. Baseline scenarios

Table 5 shows the results of optimized component sizes as well as the most important output properties for the baseline scenarios. Outcomes for component sizing can be best understood by close analysis of optimized operating strategies under the assumed technological constraints: Fig. 4 shows the normalized engine load profiles of the different cases. The mechanical efficiencies of all engines are the greatest at the highest load. As fuel costs are by far the highest cost contribution

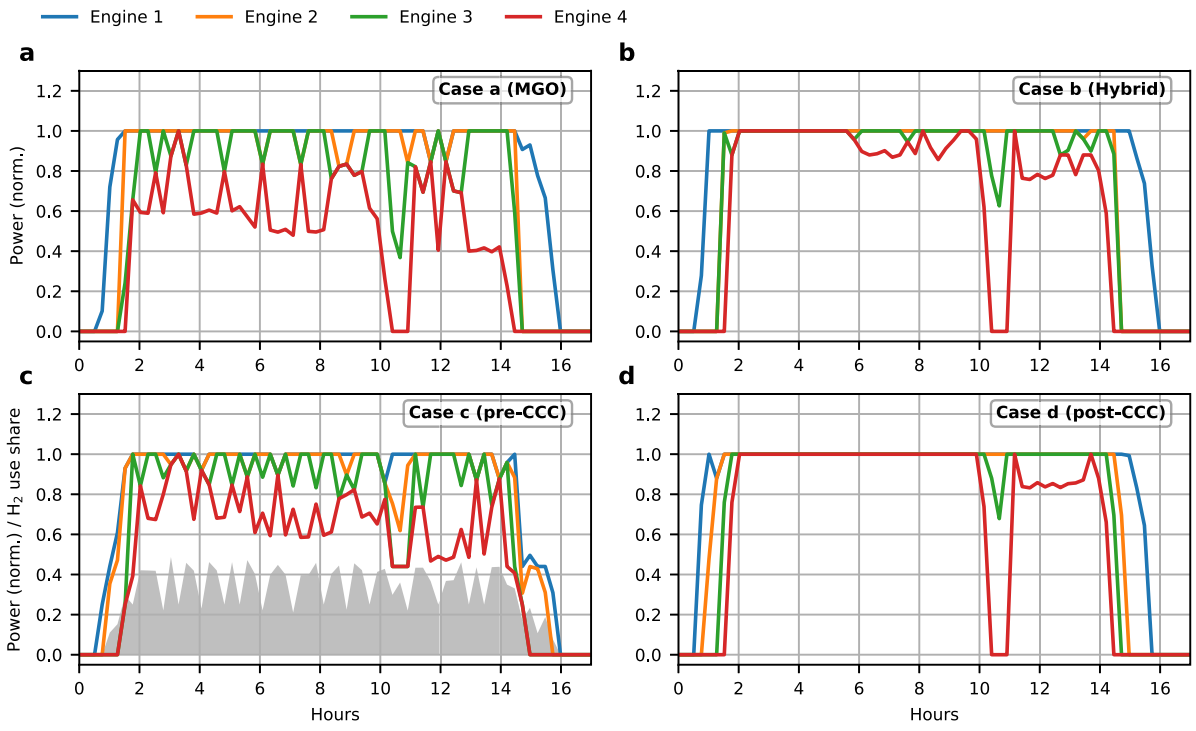


**Fig. 4.** Engine operational load profiles of the four baseline scenarios as the results of optimization. Powers are normalized to the retrieved optimization outputs (see Table 5). In panel (c), representing the pre-CCC case, the shaded area indicates the amount of $H_2$ fuel used at each time step as a share of the total installed engine power.

to the target function (see below), engines are preferably run at full load. For case a (MGO), reduced flexibility due to lack of hybridization leads to a high degree of dynamic load changes. In contrast, hybridization (case b) enables all engines to run more smoothly, and the battery buffers load operation at low efficiencies. This operation mode reduces fuel consumption and allows smaller engine sizes, which then operate at higher full load hours (Table 5). Engine operation in the post-CCC case (case d, Fig. 4d) is very similar to the hybrid case. As the amine carbon capture component also benefits from a high degree of utilization, engine load profiles are even smoother than in the hybrid case due to the use of the largest battery of all cases (see Table 5). In the pre-CCC case (case c, Fig. 4c), engines operate more dynamically because of larger thermal efficiencies at engine part loads, which can increase the available thermal energy flow to the reformer and the total system efficiency, despite lower mechanical efficiencies. Fig. 4c also indicates the times during which $H_2$ is burned. In terms of total primary energy, only 41% of engine output is provided by $H_2$. This low utilization results from non-sustainable MeOH-to-$H_2$ reformation with the operating and boundary conditions chosen in the baseline scenario. The thermal energies of the engine exhaust are not high enough to enable constant MeOH reformation, leading to a large fraction of direct MeOH combustion during operation. There are never more than two engines running on $H_2$ at the same time, and fuel switches between MeOH and $H_2$ occur very frequently. The low degree of thermal energy supply is also expressed in the dimensioning of the reformer. The optimized 11.82 $MW_{MeOH}$ correspond to a maximum capture rate of only 2.79 $t_{CO_2}$/h, compared to a capture rate of 8.53 $t_{CO_2,out}$/h in the post-CCC case (case d). Fig. 5 shows time-resolved capture rates of the membrane reformer and the amine carbon capture component. Both are optimized to run on full load as much as possible to enable a high degree of $CO_2$ capture. As carbon capture depends on the thermal output of engines, its operation closely follows the aggregated engine load profile.

Fig. 6 shows the charge states of all storage units involved in cases c and d. As expected, MeOH and $CO_2$ tank levels complement each other, and tank sizes are dimensioned just right to store the accumulated

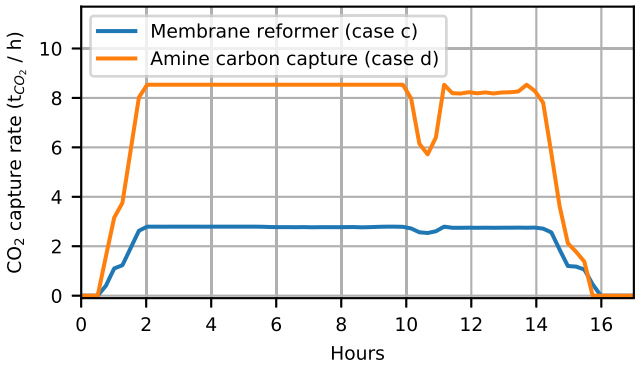


**Fig. 5.** Operational profiles of the membrane reformer and the amine carbon capture component.

liquids. The $H_2$ tank in case c has highly transient levels and is charged and discharged by switching between phases of increased MeOH and $H_2$ combustion, respectively. The optimized tank size of 1.87 MWh (Table 5), however, is very small, indicating only limited buffer function, and most $H_2$ is directly supplied to the engines without intermediate storage. In all cases, the battery is charged in the beginning so it is able to supply the occurring peak load at 3.25 h voyage length. In the pre-CCC case (case c), hardly any battery operation occurs in the rest of the voyage. Flexibility is provided by flexible engine operation (cf. Fig. 4c), which is favored due to the aforementioned increased thermal efficiency at lower loads. In the post-CCC case (case d), battery operation is more pronounced throughout the voyage because the stored energy allows the engines to run with higher mechanical efficiency more often. For example, minor changes in the total propulsion demand lead to discharging and subsequent charging between 3–6 h and 6–8 h of voyage duration, respectively. Note that the battery charge profile of the hybrid case (case b, not shown) is very similar to that of the post-CCC case (case d).

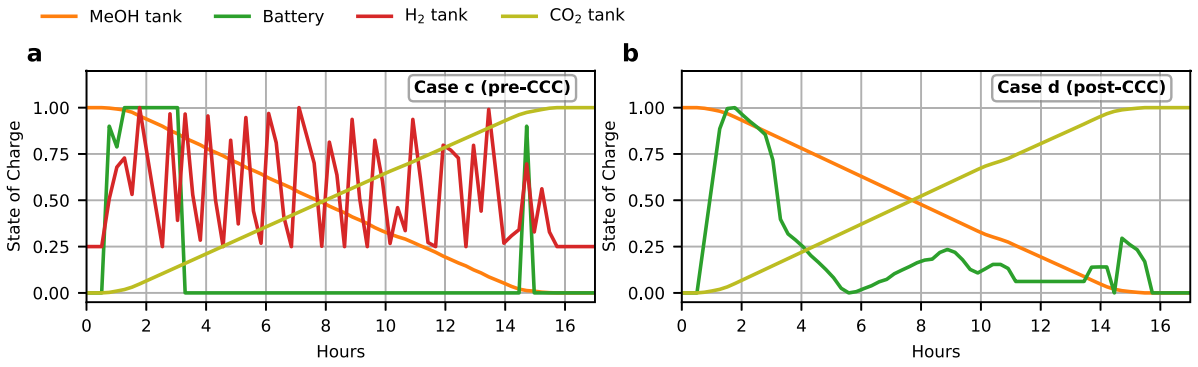


**Fig. 6.** State of charges during operation for the storage units used in the pre-CCC case (a) and the post-CCC case (d).

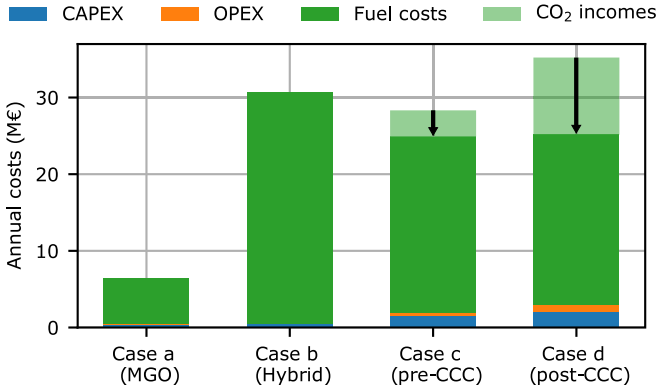


**Fig. 7.** Total costs of the baseline scenario cases and cost contributions of CAPEX, OPEX, and fuel costs. For cases c and d, the total bar height marks the costs without savings from captured $CO_2$; the latter is represented by shaded areas and downward arrows to indicate actual annual costs.

Fig. 7 shows the annual costs of all cases in the baseline scenario. Different cost contributions are indicated including investment costs (CAPEX), operating costs (OPEX) and fuel costs. All cases based on MeOH (b, c, and d) are far more expensive than the baseline case with MGO. In all cases the largest cost contribution is made by fuel costs. Comparison of the MeOH cases reveals that the carbon capture options have lower costs than the simple MeOH hybrid. In Fig. 7, the cost-reducing effect of cases c and d through saved $CO_2$ costs is indicated by downward arrows. Especially in the post-CCC case (case d), the $CO_2$ cost savings greatly reduce overall costs, overcompensating for higher investment and operating costs as well as higher fuel consumption. The cost savings compared to the MeOH hybrid case are 18.8% and 18.6% in the pre-CCC case and the post-CCC case, respectively. Thermal energies in the post-CCC case are high enough to fully utilize the carbon capture equipment, leading to a total $CO_2$ capture efficiency of 90.0%, which is the maximum that is technologically possible. In contrast, the pre-combustion carbon capture case (case c) has a much lower total capture efficiency of only 37.3%. Yet due to higher energy efficiencies, case c achieves a cost level similar to that of case d. Even if cost savings through $CO_2$ capture are not taken into account, pre-CCC costs are still lower than in the hybrid case (case b).

### 3.2. Sensitivity: renewable methanol cost

In the following sensitivity scenarios, each application case is again optimized in terms of both component design and operation. The results can be regarded as ideal configurations for the imposed and changed boundary conditions.

To test the sensitivity when the cost of renewable fuel varies all cases that use Re-MeOH are investigated in a Re-MeOH price range between 90 and 270 €/MWh. The $CO_2$ cost is kept constant at 250 €/$t_{CO_2}$ as in the baseline scenario. This sensitivity analysis can be seen as a variation of non-$CO_2$ costs in Re-MeOH synthesis including renewable energy or $H_2$ synthesis. The $CO_2$ cost reflects the cost of onshore carbon capture as part of the synthesis process and not directly a carbon tax. To better compare the scenarios to the fossil baseline, this analysis includes an additional MGO case with a fictitious $CO_2$ tax. This tax is assumed to have the same value as the $CO_2$ feedstock cost, reflecting a fictional balanced carbon market where long-term carbon sequestration compensates for fossil $CO_2$ emissions. The price therefore reflects carbon capture and transport but not storage costs. The $CO_2$ cost as a share of the total Re-MeOH cost lies between 70% and 23%, for 90 and 270 €/MWh, respectively. Fig. 8a shows the total annual costs of all scenarios and use cases. For all Re-MeOH prices, the optimizer chooses to use onboard carbon capture, exemplified by the non-zero captured $CO_2$ amounts (Fig. 8b). The carbon capture cases have economic advantages over the hybrid case throughout the entire price range. For the two lowest Re-MeOH costs, even lower annual costs than those of the MGO case can be reached if $CO_2$ costs are included. In the pre-CCC case, $CO_2$ capture increases at lower Re-MeOH prices, which can be explained by the oversized engines and the acceptance of an overall less energy-efficient design. As is shown in Fig. 8b, the total amount of captured $CO_2$ with the lowest Re-MeOH costs is around 56%, compared to a maximum 37% for higher Re-MeOH costs. Larger engine sizes result in increased fuel consumption due to operation at lower mechanical efficiencies, but increased carbon capture as a consequence of greater availability of thermal energy (Fig. 3). At low Re-MeOH prices, the post-combustion capture case has economic advantages over the pre-CCC case because of the higher capture rate and a high share of $CO_2$ in total costs. When Re-MeOH prices are high, pre-combustion carbon capture becomes the more economical choice as the increased total efficiency and therefore lower fuel consumption compensate for lower capture rates.

### 3.3. Sensitivity: Carbon dioxide cost

The overall economic performance of closed-cycle carbon capture systems is contingent on the ability to reduce $CO_2$ costs during MeOH synthesis. $CO_2$ costs depend on the main carbon source (e.g., air or biomass), available transportation infrastructure [74], or the general use of $CO_2$ as a raw material in the chemical industry [75], which affects the overall market for $CO_2$. A sensitivity analysis is therefore performed in which the $CO_2$ cost varies from 50 to 450 €/$t_{CO_2}$ at a constant non-$CO_2$ fuel price of 118 €/MWh, which corresponds to the baseline scenario. The price range resembles a $CO_2$ cost share of between 10 and 49% of total Re-MeOH costs.

Figs. 9a and Fig. 9b show the annual costs in relation to their different $CO_2$ costs and the influence on the total amount of $CO_2$ captured, respectively. Whereas the post-CCC case is not economically feasible for the lowest $CO_2$ costs, the pre-CCC case has lower costs than the MeOH

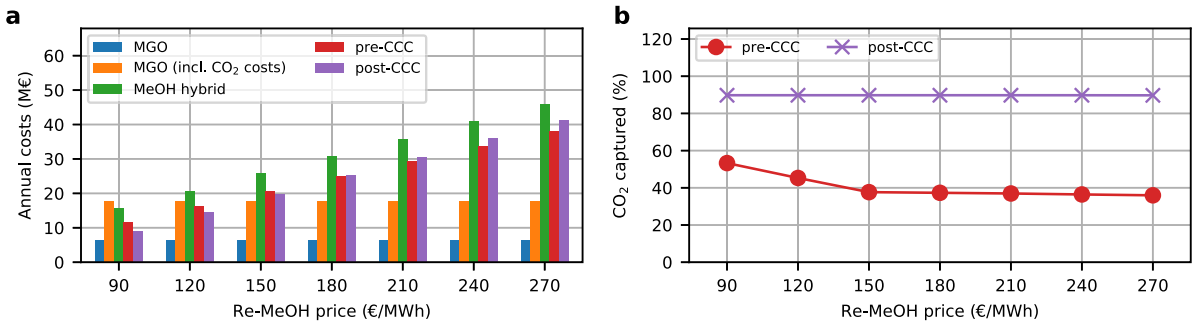


**Fig. 8.** Sensitivity analysis regarding different Re-MeOH prices. The $CO_2$ cost is kept constant at 250 €/$t_{CO_2}$. Panel (a) shows the annual costs of the different cases and panel (b) the corresponding amounts of total $CO_2$ capture.

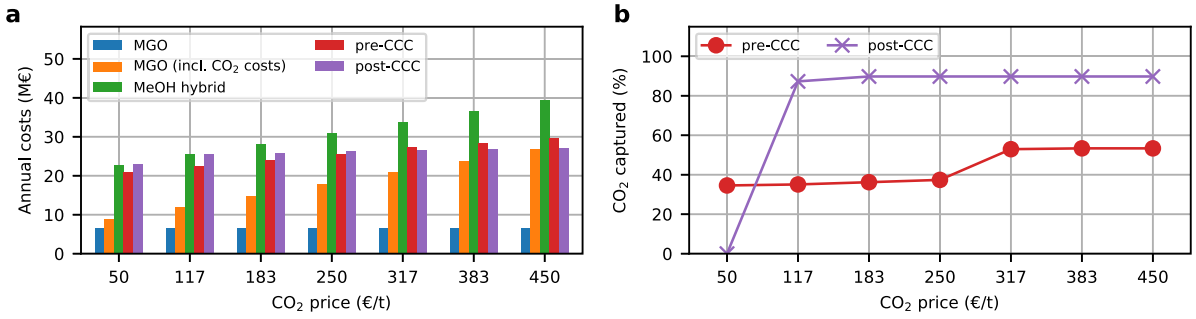


**Fig. 9.** Sensitivity analysis regarding different $CO_2$ cost shares on the total Re-MeOH costs. Panel (a) shows the annual costs for the different cost scenarios, and panel (b) the amounts of total $CO_2$ capture.

hybrid for all cost shares. At the highest $CO_2$ costs, carbon capture cases reach cost parity with the MGO case if $CO_2$ costs are included. At high $CO_2$ prices (≥317 €/$t_{CO_2}$), less energy efficient designs are again suggested in the pre-CCC case, leading to higher amounts of $CO_2$ capture. Comparing the two carbon capture alternatives, pre-CCC has lower economic costs than post-CCC at low $CO_2$ prices, whereas the reverse is true at higher $CO_2$ prices. As the non-$CO_2$ costs for Re-MeOH are kept constant in this sensitivity case, this trend can again be explained by the increasing $CO_2$ cost share at higher $CO_2$ costs, which favors the option with higher capture rates.

### 3.4. Sensitivity: improved reformer heat integration

In the baseline scenario the case of pre-combustion carbon capture (pre-CCC, case c) only achieves a total $CO_2$ capture rate of around 37% of the total carbon content in MeOH. This low capture rate is due to the low thermal exhaust energy output in combination with the high temperature heat demand of the membrane reformer. It is therefore tested whether optimization of engine operation and reformer requirements may result in sustainable reformer operations that $H_2$ combustion and generation are balanced and higher $CO_2$ capture rates can be achieved. The thermal output of an engine is a function of the available exhaust gas temperatures of the representative gas engines (see Section 2.2.1). However, engines usually offer some flexibility in the tuning of operation conditions to use more thermal energy. For example, increased exhaust gas temperatures can be reached through changed ignition timings at the expense of mechanical output power as well as through changes in the compression ratio or excess air ratio. Since the economic benefits of onboard carbon capture are due to reduced Re-MeOH costs through $CO_2$ savings, increasing thermal efficiencies could enhance overall economic performance. Whether such a strategy is economically viable in the chosen system depends on the interplay between increased costs through increased fuel consumption and decreased costs through enhanced $CO_2$ capture. To test this influence, the energy balance is systematically shifted from mechanical to thermal energy output. Mechanical (thermal) efficiencies (Fig. 3) are artificially shifted up (down) and the carbon capture cases are optimized for these altered engine performances. It is noted that it is not important how the engine operating conditions are altered. The respective changes could also be seen as introducing a virtual electric boiler with 100% efficiency, which provides thermal energy by using electricity generated by the engine. In terms of total system efficiency, however, such a strategy will always lead to increased fuel consumption as the additional electricity must be produced by the engine with its limited mechanical efficiency. Converting thermal to chemical energy, the reforming process is also not 100% efficient. There may be more sophisticated ways to increase engine exhaust gas temperatures and thus thermal efficiency without an equally strong reduction in mechanical energy output, but the described approach allows systematic study of the effects of efficiency changes without any need for more detailed engine models.

Since the available thermal engine output also depends on the necessary reformer temperature level, this scenario is tested at a multitude of reformer temperatures by assuming lower acceptable exhaust gas temperatures ($T_{exh,low}$, see Eq. (14)). This strategy corresponds to the assumption of reformer operation at lower catalyst temperatures, or more efficient use of exhaust gas heat. As listed in Table 2 no other reformer parameters are directly altered; only the useful engine thermal output is affected.

Fig. 10 shows the performance of the altered scenarios with respect to annual costs (Fig. 10a) and total $CO_2$ capture achieved (Fig. 10b). As can be seen in Fig. 10b, higher thermal efficiencies in combination with reduced reformer temperatures (reduced $T_{exh,low}$) can achieve very high capture rates, even up to the imposed technological maximum of 95%. At such an operating point, 100% $H_2$ operation is also achieved, and the reformation of Re-MeOH to $H_2$ is self-sustaining. Fig. 11 shows the engine operational profiles of the case with the maximum shifted efficiency and the lowest $T_{exh,low}$ of 200 °C. $H_2$ fuel shares at all time steps are indicated. Compared to the operation shown in Fig. 4c, $H_2$ utilization has significantly increased and the engines run at higher

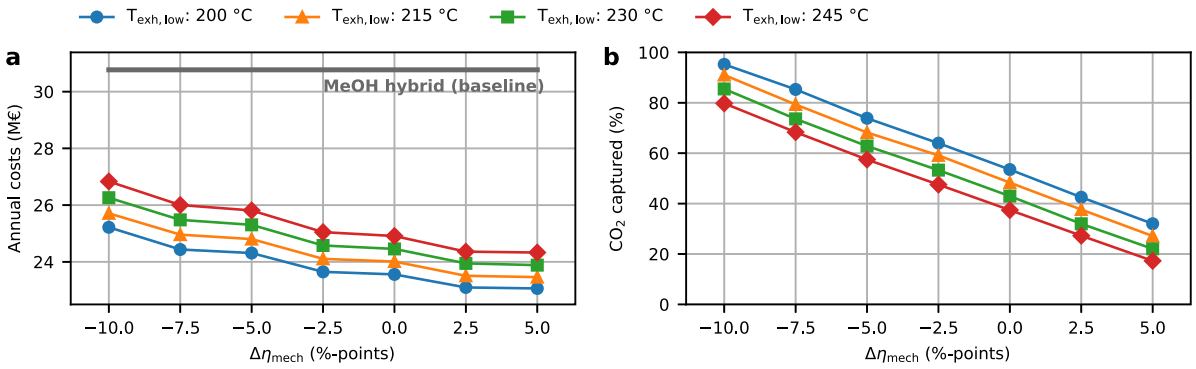


**Fig. 10.** Sensitivity analysis regarding improved heat integration in case c. Panel (a) shows annual costs as a function of efficiency changes at different exhaust gas temperature levels (reformer temperatures). Panel (b) shows the corresponding total $CO_2$ capture quantities.

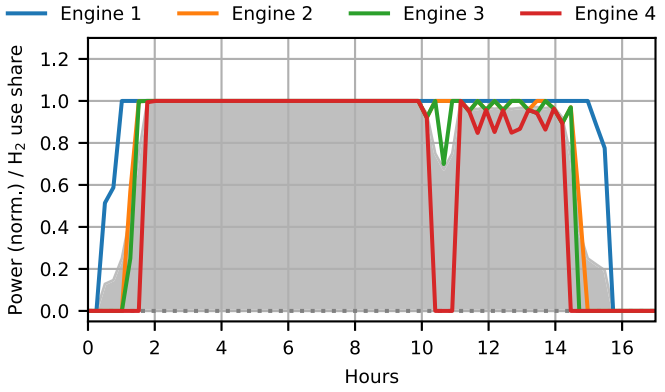


**Fig. 11.** Normalized engine operational profiles of a sensitivity case with full sustainable $H_2$ operation. $T_{exh,low}$ was tuned to 200 °C and $\Delta\eta_{mech}$ was −10%-points. The shaded area indicates the amount of $H_2$ fuel used as a share of total installed engine power.

**Table 6**
Changed parameters for improved and worsened performance scenarios for the two carbon capture cases and comparison of the total annual costs and $CO_2$ capture rates.

| | Improved | Baseline | Worse |
|---|---|---|---|
| Pre-combustion CC | | | |
| Energy demand ($kWh_{therm}/kWh_{MeOH}$) | 0.20 | 0.25 | 0.30 |
| Capture efficiency (%) | 99 | 95 | 80 |
| CAPEX (€/$kW_{MeOH}$) | 349 | 520 | 690 |
| Annual costs (M€) | 23.43 | 24.91 | 25.95 |
| $CO_2$ captured (%) | 85.3 | 37.5 | 25.0 |
| Post-combustion CC | | | |
| Energy demand ($kWh_{therm}/kg_{CO_2}$) | 0.80 | 0.85 | 0.95 |
| Capture efficiency (%) | 92 | 90 | 75 |
| CAPEX (€/$kg_{CO_2}$/h) | 1600 | 2200 | 2800 |
| Annual costs (M€) | 24.76 | 25.22 | 27.14 |
| $CO_2$ captured (%) | 92.0 | 90.0 | 72.6 |

loads and therefore higher mechanical efficiencies. Yet in terms of total fuel consumption and system efficiency, there is no improvement over the baseline scenario, exemplified by an optimized MeOH tank size of 478.4 MWh, compared to 406.9 MWh for the baseline scenario (Table 5). Higher fuel consumption also results in higher total costs for shifted efficiency scenarios (Fig. 10a). Economic savings through improved $CO_2$ capture cannot compensate for the overall efficiency decrease. However, the cost increase for lower mechanical efficiencies is only around 8%. With different $CO_2$ and Re-MeOH cost shares, engine tuning to such operating conditions might still become preferable (see Sections 3.2 and 3.3). On the contrary, reduced reformer temperature levels clearly decrease annual costs due to improved capture rates with all efficiency settings. Compared to cases with no carbon capture equipment (case b, Re-MeOH hybrid), the annual costs are lower with all efficiency settings (Fig. 10a).

### 3.5. Sensitivity: changed carbon capture performance

The carbon capture technologies described in this paper are not yet fully mature technologies, especially for mobile applications. Whereas post-combustion carbon capture is deployed in many stationary onshore applications, methanol steam reformation in a membrane reactor must evolve to be more than just a laboratory demonstration. The technological and economic parameters are prone to uncertainties, and sensitivities for improved and worsened performance scenarios are investigated (see Table 6). Altered parameters include capture efficiencies, investment costs, and thermal energy demands for the respective processes. The magnitudes of changes partly reflect ranges found in the literature; otherwise, they are chosen based on subjective assessments. In each scenario, all three parameters are changed at the same time. Especially the thermal energy demands might depend on specific temperature levels, efficient heat exchanger designs, and the use of as much internal heat redistribution as possible. The achievable maximum capture rates are a function of not only the necessary heat duty but also the choice of solvents or partial pressures of gases.

Table 6 lists total annual costs and capture efficiencies of the altered performance scenarios. In the pre-CCC case, the improved performance drastically increases total $CO_2$ capture from 37.5% to 85.3% and strongly decreases annual costs. In the post-CCC case, the total $CO_2$ capture rate closely follows the imposed capture efficiency of the amine capture component, and economic performance is only slightly enhanced. The worsened performances yield significantly lower $CO_2$ capture in the pre-CCC case (25%) and higher annual costs in both capture cases. However, annual costs are still 16% and 12% below the baseline MeOH hybrid results (case b) in the pre-CCC case and in the post-CCC case, respectively. This compares to a cost saving of 19% for both cases in the baseline scenarios. Therefore, substantial economic advantages remain even with drastic performance decreases in achievable capture rates.

## 4. Discussion

Techno-economic optimization and assessment of the two investigated options for closed-cycle onboard carbon capture clearly demonstrate that such strategies can be viable options for a fossil fuel-free shipping application. For the chosen scenarios, annualized cost savings of nearly 20% compared to a Re-MeOH system without carbon capture can be reached. The savings are a consequence of fuel cost reduction as a result of lower $CO_2$ purchase, which overcompensates for the higher investment costs. In addition, the pre-CCC case (case c) benefits from

increased efficiency based on the use of thermal engine energy for fuel production. The improved economic performance is robust against changes in Re-MeOH costs and $CO_2$ costs. Only in the post-CCC case at the lowest $CO_2$ costs does the investment required to install additional components become unfavorable. In contrast, even less energy efficient designs become acceptable at high $CO_2$ costs. Furthermore, significant cost savings are achieved compared to the simple hybrid Re-MeOH case.

Even though both carbon capture options have economic advantages, high capture rates in the baseline scenarios are only possible in the post-CCC case. In the pre-CCC case, the necessary high reforming temperature and thermal energy demands lead to only 37% carbon capture in the baseline scenario, and the system must often resort to direct Re-MeOH combustion to deliver the required propulsion demand. However, sustainable $H_2$ operation can be reached in scenarios with lower reformer temperature levels and increased thermal engine output. These results demonstrate that when carbon capture rates are high, it is crucial to closely align engine thermal outputs with reformer heat requirements. Thermal energy demands on catalytic reformers must be as low as possible to maintain high MeOH conversion and $H_2$ separation. This study assumes a newly installed system with highly efficient four-stroke engines and fixed thermal energy output. Exhaust gas temperatures in the post-CCC case are sufficient and are lower than in the pre-CCC case. In comparison, studies that previously assessed post-CCC often evaluated retrofit solutions on systems using two-stroke engines, which in general deliver lower exhaust heat enthalpies. In consequence, high capture rates could only be achieved by using additional heat sources, e.g., boilers [10,13,17], which are not necessary for the post-CCC case in this study. As illustrated by the pre-CCC case, however, it is clear that high exhaust gas temperatures are required for application of methanol steam reformation.

Studies focusing on post-CCC integration into LNG-fueled vessels often use the latent heat of LNG to liquefy $CO_2$ [14,16,76]. Since this option is not available for liquid fuels like Re-MeOH, an electric chiller was chosen for the described case study. However, it might also be feasible to use an absorption chiller that exploits waste heat from the engine cooling circuits. This thermal energy is usually used to supply hotel heat loads, especially during the cold season. Whereas the current study only focuses on supplying the propulsion load, future studies should also consider such hotel loads, including electricity demand, to obtain a comprehensive design of the overall energy system.

The investigated scenarios assume the use of highly mature technologies, e.g., MeOH and $H_2$ engines with high efficiencies, as well as high capture rates of carbon capture components. Sensitivities with lower carbon capture efficiencies and reduced mechanical efficiency in the $H_2$ engine still deliver cost advantages compared to a system without carbon capture. In the pre-CCC case, increased thermal energy output at the cost of mechanical output could even be beneficial for sustainable reformer operation, leading to higher capture rates. Nevertheless, first (onboard) technology demonstrators will have to prove feasibility before final assertions can be made. Due to the optimization-based nature of the assessments, component dimensions are optimized to exactly match the desired demand profile (Fig. 2). A final system design must be able to cover various different propulsion profiles, and some degree of oversizing should be taken into account.

Although economic performance might favor the application of closed-cycle onboard carbon capture, several major issues not directly related to costs could hinder the approach: The installation of a complex $CO_2$ handling system on board results in increased technological know-how as well as safety requirements that ship operators will have to meet. Space requirements for the carbon capture components and $CO_2$ tanks will reduce the amount of usable cargo space. In future models, this issue could be addressed by adding the cost of lost cargo for each component into economic target functions, as attempted by Korberg et al. [20] in their techno-economic assessment. Furthermore, the feasibility of an onboard carbon capture system rests upon $CO_2$ bunker and transportation infrastructure being available at the port of departure and destination. The availability of such $CO_2$ infrastructure might largely depend on the overall market penetration of $CO_2$, both for carbon storage and for utilization in the chemical industry. It would be helpful for ports to become centers of big industrial net-zero hubs, where infrastructure for carbon capture, renewable fuel imports, and large industrial consumers are aggregated [77]. Both the question of reduced cargo space and available fuel structure will be able to be incorporated into the model used in this paper.

The availability of $CO_2$ port infrastructure will also decide whether closed-cycle onboard carbon capture concepts can be extended to a multitude of other ship types, for example larger carriers or container vessels. This study selected a ferry as the system of choice because it is most likely that the $CO_2$ handling system would first be used on a fixed route with only two ports. If the propulsion concept allows the use of sufficient thermal energy in the process, the chosen concepts may be transferred to other vessels. However, economic advantages might still be limited to applications where fuel costs make up the largest share of net annual costs.

The results show that the use of carbon capture can become a lower cost option than the simple use of Re-MeOH in internal combustion engine (ICE) based propulsion. However, there are several other zero-emission shipping options that might be adopted by the maritime industry including ammonia, biofuels, (liquid) hydrogen, and synthetic fuels, all of which may be used both in ICE and fuel cells. A comparison with these technologies at the same level of detail goes beyond the scope of this article, and the reader is referred to references that provide broader techno-economic and life cycle assessments [20–23]. However, detailed modeling of onboard energy systems can provide useful inputs for such calculations. For example, previous assessments of the HyMethShip pre-CCC concept performed by Malmgren et al. [7] used data from the specific engine developed in the project that was tuned for high exhaust gas heat, ensuring sufficient heat for full $H_2$ operation during cruising. In contrast, the system in this publication resulted in only partial $H_2$ operation and limited carbon capture due to its use of more detailed technological constraints and cost optimization of the onboard energy system. The proposed method for techno-economic assessment could be used first to optimize the propulsion system and then to take these results as input for life cycle performance analysis. The entire renewable fuel production chain might be included in the model as a further improvement and complete assessment. Whereas the main target of the optimization approach is to test the techno-economic feasibility of the concepts, results inherently also include an optimized operation. For a previously selected layout, these trajectories could be used to deliver important insights into optimal operational control. As the demand profile must be known in advance, the model is ideally suited to be combined with predictive control strategies [78], for example where weather and route prediction serve as input and optimal component deployment is suggested by the optimizer.

## 5. Conclusion

This paper analyzes a ship energy system based on the renewable fuel methanol in combination with different forms of onboard carbon capture by means of techno-economic optimization. The time-resolved nature of the optimization model allowed the analysis of best-case designs that consider operation during a complete trip of a ferry operating in the Baltic Sea. The results show that designs with optimal costs may be achieved with both pre-combustion and post-combustion carbon capture technology, delivering annual cost advantages of about 20% over a system without carbon capture. Whereas the engine heat supply of the chosen post-combustion configuration is sufficient to enable high capture rates of 90%, the pre-combustion capture rate is limited to about 37% due to the high temperature demanded by the methanol reformer. However, higher capture rates up to the imposed technological

maximum of 95% can be achieved for increased engine exhaust energies. A more detailed assessment of thermal energy supply including additional heat sources such as fuel burners should enable cost-effective operation while keeping capture rates high. Key uncertainties that remain are future developments in fuel costs and especially $CO_2$ costs as well as technology performance. Although these factors influence the economic outcome, the overall advantage of onboard carbon capture remains robust, as demonstrated by detailed sensitivity analysis. The results presented here offer insights into onboard combustion and $CO_2$ capture as two parts of a more extended closed carbon cycle that includes port infrastructure, $CO_2$ transportation and renewable fuel synthesis. Future studies should apply the proposed methods to assess this complete cycle. In addition, other onboard energy demands such as hotel loads and non-energy system-related integration issues such as space requirements and weight increases might be addressed.

## CRediT authorship contribution statement

**Bernhard Thaler:** Conceptualization, Data curation, Investigation, Methodology, Visualization, Interpretation, Writing – original draft, Review & editing. **Fayas Malik Kanchiralla:** Data curation, Interpretation, Review & editing. **Stefan Posch:** Conceptualization, Supervision, Interpretation, Review & editing. **Gerhard Pirker:** Conceptualization, Funding acquisition, Project administration, Supervision, Interpretation, Review & editing. **Andreas Wimmer:** Funding acquisition, Interpretation, Review & editing. **Selma Brynolf:** Conceptualization, Funding acquisition, Project administration, Supervision, Interpretation, Review & editing. **Nicole Wermuth:** Conceptualization, Funding acquisition, Project administration, Supervision, Interpretation, Review & editing.

## Declaration of competing interest

The authors declare that they have no known competing financial interests or personal relationships that could have appeared to influence the work reported in this paper.

## Data availability

Data will be made available on request.

## Acknowledgments

B.T., S.P., G.P., A.W. and N.W. would like to acknowledge the financial support of the “COMET — Competence Centres for Excellent Technologies” Programme of the Austrian Federal Ministry for Climate Action, Environment, Energy, Mobility, Innovation and Technology (BMK) and the Federal Ministry for Digital and Economic Affairs (BMDW), Austria and the Provinces of Styria, Tyrol and Vienna for the COMET Centre (K1) LEC EvoLET. The COMET Programme is managed by the Austrian Research Promotion Agency (FFG). F.K. and S.B. would like to acknowledge the financial support of the Swedish Transport Administration’s industry program Sustainable shipping led by the Swedish Maritime Competence Centre (Lighthouse), grant number FS_E_2021 Carbon capture potential on-board ships and the European Union’s Horizon 2020 Research and innovation program under grant agreement No 768945. We acknowledge Stena Teknik for providing data for the study.

## References

[1] Balcombe P, Brierley J, Lewis C, Skatvedt L, Speirs J, Hawkes A, Staffell I. How to decarbonise international shipping: Options for fuels, technologies and policies. Energy Convers Manage 2019;182:72–88. http://dx.doi.org/10.1016/j.enconman.2018.12.080.

[2] Bouman EA, Lindstad E, Rialland AI, Strømman AH. State-of-the-art technologies, measures, and potential for reducing GHG emissions from shipping – A review. Transp Res D 2017;52:408–21. http://dx.doi.org/10.1016/j.trd.2017.03.022.

[3] Chryssakis C, Brinks H, Brunelli A, Fuglseth TP, Lande M, Laugen L, Longva T, Raeissi B, Tvete HA. Low carbon shipping towards 2050. Tech. rep., technical report, Høvik, Norway: DNV GL; 2017, URL https://www.dnv.com/Publications/low-carbon-shipping-towards-2050-93579.

[4] Traut M, Larkin A, Anderson K, McGlade C, Sharmina M, Smith T. $CO_2$ abatement goals for international shipping. Clim Policy 2018;18(8):1066–75. http://dx.doi.org/10.1080/14693062.2018.1461059.

[5] Eide MS, Longva T, Hoffmann P, Endresen Ø, Dalsøren SB. Future cost scenarios for reduction of ship $CO_2$ emissions. Marit Policy Manage 2011;38(1):11–37. http://dx.doi.org/10.1080/03088839.2010.533711.

[6] Yuan J, Ng SH, Sou WS. Uncertainty quantification of $CO_2$ emission reduction for maritime shipping. Energy Policy 2016;88:113–30. http://dx.doi.org/10.1016/j.enpol.2015.10.020.

[7] Malmgren E, Brynolf S, Fridell E, Grahn M, Andersson K. The environmental performance of a fossil-free ship propulsion system with onboard carbon capture–a life cycle assessment of the HyMethShip concept. Sustain Energy Fuels 2021;5(10):2753–70. http://dx.doi.org/10.1039/D1SE00105A.

[8] Hansson J, Månsson S, Brynolf S, Grahn M. Alternative marine fuels: Prospects based on multi-criteria decision analysis involving Swedish stakeholders. Biomass Bioenergy 2019;126:159–73. http://dx.doi.org/10.1016/j.biombioe.2019.05.008.

[9] Comparison of alternative marine fuels. Høvik, Norway: DNV GL; 2019, URL https://safety4sea.com/wp-content/uploads/2019/09/SEA-LNG-DNV-GL-Comparison-of-Alternative-Marine-Fuels-2019_09.pdf.

[10] Oil and Gas Climate Initiative and Stena Bulk. Is carbon capture on ships feasible? A report from the oil and gas climate initiative [online]. 2021, URL https://www.ogci.com/wp-content/uploads/2021/11/OGCI_STENA_MCC_November_2021.pdf.

[11] Value Maritime. JR shipping switches another six ships to value maritime’s advanced filter and carbon capture system [online]. 2022, URL https://valuemaritime.com/news/jr-shipping-switches-another-six-ships-to-value-maritimes-advanced-filter-and-carbon-capture-system/.

[12] Liang ZH, Rongwong W, Liu H, Fu K, Gao H, Cao F, Zhang R, Sema T, Henni A, Sumon K, et al. Recent progress and new developments in post-combustion carbon-capture technology with amine based solvents. Int J Greenh Gas Control 2015;40:26–54. http://dx.doi.org/10.1016/j.ijggc.2015.06.01.

[13] Luo X, Wang M. Study of solvent-based carbon capture for cargo ships through process modelling and simulation. Appl Energy 2017;195:402–13. http://dx.doi.org/10.1016/j.apenergy.2017.03.027.

[14] Feenstra M, Monteiro J, van den Akker JT, Abu-Zahra MR, Gilling E, Goetheer E. Ship-based carbon capture onboard of diesel or LNG-fuelled ships. Int J Greenh Gas Control 2019;85:1–10. http://dx.doi.org/10.1016/j.ijggc.2019.03.008.

[15] Long NVD, Lee DY, Kwag C, Lee YM, Lee SW, Hessel V, Lee M. Improvement of marine carbon capture onboard diesel fueled ships. Chem Eng Process-Process Intensif 2021;168:108535. http://dx.doi.org/10.1016/j.cep.2021.10853.

[16] Ros JA, Skylogianni E, Doedée V, van den Akker JT, Vredeveldt AW, Linders MJ, Goetheer EL, Monteiro JGM. Advancements in ship-based carbon capture technology on board of LNG-fuelled ships. Int J Greenh Gas Control 2022;114:103575. http://dx.doi.org/10.1016/j.ijggc.2021.103575.

[17] Einbu A, Pettersen T, Morud J, Tobiesen A, Jayarathna C, Skagestad R, Nysæther G. Energy assessments of onboard $CO_2$ capture from ship engines by MEA-based post combustion capture system with flue gas heat integration. Int J Greenh Gas Control 2022;113:103526. http://dx.doi.org/10.1016/j.ijggc.2021.103526.

[18] Kanniche M, Gros-Bonnivard R, Jaud P, Valle-Marcos J, Amann J-M, Bouallou C. Pre-combustion, post-combustion and oxy-combustion in thermal power plant for $CO_2$ capture. Appl Therm Eng 2010;30(1):53–62. http://dx.doi.org/10.1016/j.applthermaleng.2009.05.005.

[19] Zelenka J, Wermuth N, Lackner M, Wimmer A, Andersson K, Veelken H, Moeyaert P, Jäger B, Url M, Lang M, et al. The HyMethShip project: Innovative emission free propulsion for ships. In: 29th CIMAC world congress on internal combustion engines. 2019.

[20] Korberg AD, Brynolf S, Grahn M, Skov IR. Techno-economic assessment of advanced fuels and propulsion systems in future fossil-free ships. Renew Sustain Energy Rev 2021;142:110861. http://dx.doi.org/10.1016/j.rser.2021.110861.

[21] Horvath S, Fasihi M, Breyer C. Techno-economic analysis of a decarbonized shipping sector: Technology suggestions for a fleet in 2030 and 2040. Energy Convers Manage 2018;164:230–41. http://dx.doi.org/10.1016/j.enconman.2018.02.098, URL https://www.sciencedirect.com/science/article/pii/S0196890418302152.

[22] Wang Y, Wright LA. A comparative review of alternative fuels for the maritime sector: Economic, technology, and policy challenges for clean energy implementation. World 2021;2(4):456–81. http://dx.doi.org/10.3390/world2040029.

[23] McKinlay CJ, Turnock SR, Hudson DA. Route to zero emission shipping: Hydrogen, ammonia or methanol? Int J Hydrogen Energy 2021;46(55):28282–97. http://dx.doi.org/10.1016/j.ijhydene.2021.06.066.

[24] Choi BC, Kim YM. Thermodynamic analysis of a dual loop heat recovery system with trilateral cycle applied to exhaust gases of internal combustion engine for propulsion of the 6800 TEU container ship. Energy 2013;58:404–16. http://dx.doi.org/10.1016/j.energy.2013.05.017.

[25] Fathima AH, Palanisamy K. Optimization in microgrids with hybrid energy systems–A review. Renew Sustain Energy Rev 2015;45:431–46. http://dx.doi.org/10.1016/j.rser.2015.01.059.

[26] Frangopoulos CA. Developments, trends, and challenges in optimization of ship energy systems. Appl Sci 2020;10(13):4639. http://dx.doi.org/10.3390/app10134639.

[27] Baldi F, Ahlgren F, Melino F, Gabrielii C, Andersson K. Optimal load allocation of complex ship power plants. Energy Convers Manage 2016;124:344–56. http://dx.doi.org/10.1016/j.enconman.2016.07.009.

[28] Baldi F, Wang L, Maréchal Fc. Integration of solid oxide fuel cells in cruise ship energy systems. In: Proceedings of the 31st international conference on efficiency, cost, optimization, simulation and environmental impact of energy systems. 2018, URL https://infoscience.epfl.ch/record/257978.

[29] Baldi F, Brynolf S, Maréchal F. The cost of innovative and sustainable future ship energy systems, in: Proceedings of the 32nd International Conference on Efficiency, Cost, Optimization, Simulation and Environmental Impact of Energy Systems, WrocłAw, Poland, 2019, pp. 23–28.

[30] Pivetta D, Dall'Armi C, Taccani R. Multi-objective optimization of hybrid PEMFC/Li-ion battery propulsion systems for small and medium size ferries. Int J Hydrogen Energy 2021. http://dx.doi.org/10.1016/j.ijhydene.2021.02.124.

[31] Tang R, Wu Z, Li X. Optimal operation of photovoltaic/battery/diesel/cold-ironing hybrid energy system for maritime application. Energy 2018;162:697–714. http://dx.doi.org/10.1016/j.energy.2018.08.048.

[32] Bordin C, Mo O. Including power management strategies and load profiles in the mathematical optimization of energy storage sizing for fuel consumption reduction in maritime vessels. J Energy Storage 2019;23:425–41. http://dx.doi.org/10.1016/j.est.2019.03.021.

[33] Yan Y, Zhang H, Long Y, Wang Y, Liang Y, Song X, James J. Multi-objective design optimization of combined cooling, heating and power system for cruise ship application. J Cleaner Prod 2019;233:264–79. http://dx.doi.org/10.1016/j.jclepro.2019.06.047.

[34] Trivyza NL, Rentizelas A, Theotokatos G. A novel multi-objective decision support method for ship energy systems synthesis to enhance sustainability. Energy Convers Manage 2018;168:128–49. http://dx.doi.org/10.1016/j.enconman.2018.04.020.

[35] Rivarolo M, Rattazzi D, Magistri L. Best operative strategy for energy management of a cruise ship employing different distributed generation technologies. Int J Hydrogen Energy 2018;43(52):23500–10. http://dx.doi.org/10.1016/j.ijhydene.2018.10.217.

[36] Ancona MA, Baldi F, Bianchi M, Branchini L, Melino F, Peretto A, Rosati J. Efficiency improvement on a cruise ship: Load allocation optimization. Energy Convers Manage 2018;164:42–58. http://dx.doi.org/10.1016/j.enconman.2018.02.080.

[37] Tang R, Li X, Lai J. A novel optimal energy-management strategy for a maritime hybrid energy system based on large-scale global optimization. Appl Energy 2018;228:254–64. http://dx.doi.org/10.1016/j.apenergy.2018.06.092.

[38] Santos HG, Toffolo TA. Mixed integer linear programming with python. 2020.

[39] Forrest J, Ralphs T, Vigerske S, LouHafer, Kristjansson B, Fasano J, EdwinStraver, Lubin M, Santos HG, Lougee R, Saltzman M. Coin-or/cbc: Version 2.9.9. 2018, http://dx.doi.org/10.5281/zenodo.1317566.

[40] Žižlavskỳ O. Net present value approach: method for economic assessment of innovation projects. Procedia-Soc Behav Sci 2014;156:506–12. http://dx.doi.org/10.1016/j.sbspro.2014.11.230.

[41] Assaf J, Shabani B. Economic analysis and assessment of a standalone solar-hydrogen combined heat and power system integrated with solar-thermal collectors. Int J Hydrogen Energy 2016;41(41):18389–404. http://dx.doi.org/10.1016/j.ijhydene.2016.08.117.

[42] Wärtsilä 31 SG: product guide. URL https://www.wartsila.com/marine/build/engines-and-generating-sets/pure-gas-engines/wartsila-31sg.

[43] Wärtsilä 26: product guide. URL https://www.wartsila.com/marine/build/engines-and-generating-sets/diesel-engines/wartsila-26.

[44] McBride BJ. Coefficients for calculating thermodynamic and transport properties of individual species, Vol. 4513. NASA Langley Research Center; 1993.

[45] Danish Energy Agency and Energine. Technology data for industrial process heat and carbon capture. Tech. rep., Danish Energy Agency; 2020, URL https://ens.dk/sites/ens.dk/files/Analyser/technology_data_for_carbon_capture_transport_and_storage.pdf.

[46] Gabrielli P, Flamm B, Eichler A, Gazzani M, Lygeros J, Mazzotti M. Modeling for optimal operation of PEM fuel cells and electrolyzers. In: 2016 IEEE 16th international conference on environment and electrical engineering (EEEIC). 2016, p. 1–7. http://dx.doi.org/10.1109/EEEIC.2016.7555707.

[47] Beale EML, Tomlin JA. Special facilities in a general mathematical programming system for non-convex problems using ordered sets of variables. OR 1970;69(447–454):99.

[48] Dalena F, Senatore A, Basile M, Knani S, Basile A, Iulianelli A. Advances in methanol production and utilization, with particular emphasis toward hydrogen generation via membrane reactor technology. Membranes 2018;8(4):98, URL https://doi.org/10.3390/membranes8040098.

[49] Iulianelli A, Ribeirinha P, Mendes A, Basile A. Methanol steam reforming for hydrogen generation via conventional and membrane reactors: A review. Renew Sustain Energy Rev 2014;29:355–68. http://dx.doi.org/10.1016/j.rser.2013.08.032.

[50] Gorset O, Knudsen JN, Bade OM, Askestad I. Results from testing of aker solutions advanced amine solvents at $CO_2$ technology centre mongstad. Energy Procedia 2014;63:6267–80. http://dx.doi.org/10.1016/j.egypro.2014.11.658.

[51] Stec M, Tatarczuk A, Więcław-Solny L, Krótki A, Spietz T, Wilk A, Śpiewak D. Demonstration of a post-combustion carbon capture pilot plant using amine-based solvents at the łaziska power plant in Poland. Clean Technol Environ Policy 2016;18(1):151–60. http://dx.doi.org/10.1007/s10098-015-1001-2.

[52] Domenichini R, Mancuso L, Ferrari N, Davison J. Operating flexibility of power plants with carbon capture and storage (CCS). Energy Procedia 2013;37:2727–37. http://dx.doi.org/10.1016/j.egypro.2013.06.157.

[53] Decarre S, Berthiaud J, Butin N, Guillaume-Combecave J-L. $CO_2$ maritime transportation. Int J Greenh Gas Control 2010;4(5):857–64. http://dx.doi.org/10.1016/j.ijggc.2010.05.005.

[54] Øi LE, Eldrup N, Adhikari U, Bentsen MH, Badalge JL, Yang S. Simulation and cost comparison of $CO_2$ liquefaction. Energy Procedia 2016;86:500–10. http://dx.doi.org/10.1016/j.egypro.2016.01.051.

[55] Durusut E, Joos M. Element energy: Shipping $CO_2$ – UK cost estimation study. Tech. rep., Department for Business, Energy and Industrial Strategy; 2018.

[56] Vimmerstedt L. 2021 Annual technology baseline (ATB) cost and performance data for electricity generation technologies. 2021, http://dx.doi.org/10.25984/1807473.

[57] Jun P, Gillenwater M, Barbour W. $CO_2$, $CH_4$, and $N_2O$ emissions from transportation–water-borne navigation. In: Good practice guidance and uncertainty management in national greenhouse gas inventories, intergovernmental panel on climate change, Paris, France. 2000, p. 71–92.

[58] IRENA and Methanol Institute. Innovation outlook: Renewable methanol. 2021, URL https://www.irena.org/publications/2021/Jan/Innovation-Outlook-Renewable-Methanol.

[59] Livanos GA, Theotokatos G, Pagonis D-N. Techno-economic investigation of alternative propulsion plants for Ferries and RoRo ships. Energy Convers Manage 2014;79:640–51. http://dx.doi.org/10.1016/j.enconman.2013.12.0500.

[60] Lehtveer M, Brynolf S, Grahn M. What future for electrofuels in transport? Analysis of cost competitiveness in global climate mitigation. Environ Sci Technol 2019;53(3):1690–7. http://dx.doi.org/10.1021/acs.est.8b05243.

[61] Byun M, Lee B, Lee H, Jung S, Ji H, Lim H. Techno-economic and environmental assessment of methanol steam reforming for $h_2$ production at various scales. Int J Hydrogen Energy 2020;45(46):24146–58, URL https://doi.org/10.1016/j.ijhydene.2020.06.097.

[62] Malmgren E, Brynolf S, Borgh M, Ellis J, Grahn M, Wermuth N. The HyMethShip concept: An investigation of system design choices and vessel operation characteristics influence on life cycle performance. In: 8th transport research Arena. Helsinki, Finland. 2020.

[63] based on expert interviews with the HyMethShip project consortium.

[64] Schach M-O, Schneider R, Schramm H, Repke J-U. Techno-economic analysis of postcombustion processes for the capture of carbon dioxide from power plant flue gas. Ind Eng Chem Res 2010;49(5):2363–70. http://dx.doi.org/10.1021/ie900514t.

[65] Taljegard M, Brynolf S, Grahn M, Andersson K, Johnson H. Cost-effective choices of marine fuels in a carbon-constrained world: results from a global energy model. Environ Sci Technol 2014;48(21):12986–93. http://dx.doi.org/10.1021/es5018575.

[66] Knudsen J, Knudsen NO. Technology data for energy storage. Tech. rep., Danish Energy Agency; 2020, URL https://ens.dk/sites/ens.dk/files/Analyser/technology_data_catalogue_for_energy_storage.pdf.

[67] European Central Bank Eurosystem. Statistical data warehouse - economic activity. 2021, URL https://sdw.ecb.europa.eu/.

[68] Rubin ES, Davison JE, Herzog HJ. The cost of $CO_2$ capture and storage. Int J Greenh Gas Control 2015;40:378–400. http://dx.doi.org/10.1016/j.ijggc.2015.05.018.

[69] Irlam L. Global costs of carbon capture and storage. Global CCS Institute; 2017.

[70] Awoyomi A, Patchigolla K, Anthony EJ. Process and economic evaluation of an onboard capture system for LNG-fueled $CO_2$ carriers. Ind Eng Chem Res 2019;59(15):6951–60. http://dx.doi.org/10.1021/acs.iecr.9b04659.

[71] Brynolf S, Taljegard M, Grahn M, Hansson J. Electrofuels for the transport sector: A review of production costs. Renew Sustain Energy Rev 2018;81:1887–905. http://dx.doi.org/10.1016/j.rser.2017.05.288.

[72] Fasihi M, Efimova O, Breyer C. Techno-economic assessment of $CO_2$ direct air capture plants. J Cleaner Prod 2019;224:957–80. http://dx.doi.org/10.1016/j.jclepro.2019.03.086.

[73] Ragnhildur S, Akshat R. World's largest carbon-sucking plant starts making tiny dent in emissions. 2021, Bloomberg.Com. URL https://www.bloomberg.com/news/features/2021-09-08/inside-the-world-s-largest-direct-carbon-capture-plant.

[74] Knoope M, Ramírez A, Faaij A. The influence of uncertainty in the development of a $CO_2$ infrastructure network. Appl Energy 2015;158:332–47, URL https://doi.org/10.1016/j.apenergy.2015.08.024.
[75] Kaiser S, Bringezu S. Use of carbon dioxide as raw material to close the carbon cycle for the German chemical and polymer industries. J Cleaner Prod 2020;271:122775. http://dx.doi.org/10.1016/j.jclepro.2020.122775.
[76] Monteiro J. CO2ASTS – carbon capture, storage and transfer in shipping a technical and economic feasibility study: Public concise report. 2020, URL https://www.mariko-leer.de/wp-content/uploads/2020/06/200513-CO2ASTS-Public-Concise-Report.pdf.
[77] Friedmann J, Agrawal M, Bhwardwaj A. Evaluation net-zero industrial hubs in the United States: a case study of houston. 2021, URL https://energypolicy.columbia.edu/sites/default/files/file-uploads/Houston%2C%20final%20design%2C%206.29.21.pdf.
[78] Hu J, Shan Y, Guerrero JM, Ioinovici A, Chan KW, Rodriguez J. Model predictive control of microgrids–An overview. Renew Sustain Energy Rev 2021;136:110422. http://dx.doi.org/10.1016/j.rser.2020.110422.